

# A Distributed Lagrange Multiplier Based Fictitious Domain Method for Maxwell's Equations

V. A. Bokil<sup>a</sup> and R. Glowinski<sup>b</sup>

Center for Research in Scientific Computation<sup>a</sup>  
North Carolina State University  
Box 8205  
Raleigh, NC 27695-8205

Department of Mathematics<sup>b</sup>  
University of Houston  
Houston, TX 77204

January 19, 2006

## Abstract

We consider a time-dependent problem of scattering by an obstacle involving the solution of the two dimensional Maxwell's equations in the exterior of a domain with a perfectly conducting condition on the boundary of this domain. We propose a novel fictitious domain method based on a distributed Lagrange multiplier technique for the solution of this problem. Perfectly matched layers are constructed to model the unbounded problem. Comparisons are performed with the finite difference scheme, that demonstrate the advantages of our fictitious domain method over the staircase approximation of the finite difference method. We conclude that our distributed multiplier approach is a simple, effective and far more accurate alternative to the popular FDTD method for solving Maxwell's equations.

*Keywords:* Fictitious domains, Perfectly matched layers, Mixed finite element methods, FDTD, Maxwell's equations.

<sup>a</sup>vabokil@ncsu.edu

<sup>b</sup>roland@math.uh.edu

# 1 Introduction

Electromagnetic phenomena play an important role in modern technology in different areas such as advanced mobile information systems, the design, development, integration, and testing of antennas, communication signal processing and many more. Applications involve the propagation and scattering of transient electromagnetic signals such as in aircraft radar signature analysis or the nondestructive testing of concrete structures. The study of such applications requires the ability to predict different kinds of electromagnetic effects. Some of the important effects include the radar scattering attributes i.e., radar cross section (RCS) of different complex objects such as airplanes and missiles, the propagation of pulses through dispersive media such as soil or concrete to detect pollutants or hidden targets, interaction of electromagnetic waves with biological media, the interaction of antenna elements with aircrafts and ships, and many more [23].

The complete set of laws for time-varying electromagnetic phenomena can be derived from physical concepts such as electric charges and current density, some universal laws, such as the conservation of electric charge, Faraday's and Ampere's laws, and constituent laws which are characteristic for a given medium [11]. These laws of electromagnetism are represented by *Maxwell's equations* and are central to predictions such as those described in the paragraph above. There are many different techniques available for solving the time-dependent problem of scattering by an obstacle, including finite difference and finite element methods. In [5] we introduced a fictitious domain method, based on a distributed Lagrange multiplier, for the solution of the two-dimensional scalar wave equation with a Dirichlet condition on the boundary of an obstacle. In this paper we will discuss how the distributed Lagrange multiplier fictitious domain formulation employed in [5] can be applied to the case of the two-dimensional TM mode of Maxwell's equations.

A fictitious domain method is a technique in which the solution to a given problem is obtained by extending the given data to a larger but simpler shaped domain, containing the original domain, and solving corresponding equations in this larger *fictitious domain*. Let  $\Omega \subset \mathbb{R}^d$  ( $d = 1, 2, 3$ ) be a domain which contains an inclusion  $\omega$  as shown in Figure 1. We consider solving for  $\Phi$  in a boundary value problem of the type

$$\begin{aligned} A(\Phi) &= f, \text{ in } \Omega \setminus \bar{\omega}, \\ B_{\Gamma}(\Phi) &= g_0, \text{ on } \Gamma = \partial\Omega, \\ B_{\partial\omega}(\Phi) &= g_1, \text{ on } \partial\omega, \end{aligned} \tag{1.1}$$

where the functions  $f, g_0, g_1$  and the operators  $A, B_{\Gamma}, B_{\partial\omega}$ , are known. In a fictitious domain approach we replace (1.1) by another problem of the type

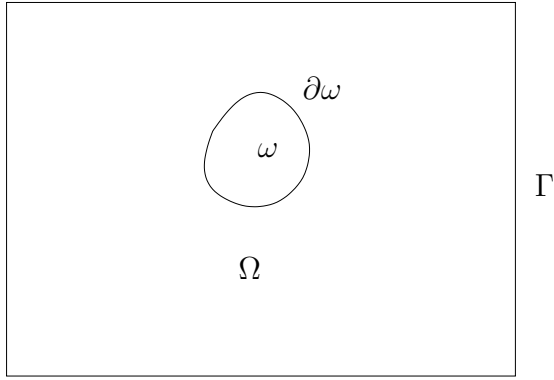


Figure 1: The obstacle  $\omega$  embedded inside the larger domain  $\Omega$ .

Find  $\phi$  defined over  $\Omega$  and  $M_\gamma$  a measure supported by  $\partial\omega$ , so that

$$\begin{aligned}
 \text{(i)} \quad & \tilde{A}(\phi) = \tilde{f} + M_\gamma, \text{ in } \Omega, \\
 \text{(ii)} \quad & \tilde{B}_\Gamma(\phi) = g_0, \text{ on } \Gamma = \partial\Omega, \\
 \text{(iii)} \quad & \tilde{B}_{\partial\omega}(\phi|_{\Omega \setminus \bar{\omega}}) = g_1, \text{ on } \partial\omega,
 \end{aligned} \tag{1.2}$$

where the operator  $\tilde{A}$  is of the same type as  $A$  and coincides (in some sense) with  $A$  on  $\Omega \setminus \bar{\omega}$ ,  $\tilde{f}$  is some extension of  $f$  over  $\Omega$  and  $\tilde{B}_\Gamma$ , and  $\tilde{B}_{\partial\omega}$  are extensions of  $B_\Gamma$ , and  $B_{\partial\omega}$ , respectively. If we choose the measure  $M_\gamma$  so that the solution of (1.2,i,ii) satisfies relation (1.2,iii) then we can expect to have  $\phi|_{\Omega \setminus \bar{\omega}} = \Phi$ . If  $\Omega$  has a simple shape such as a rectangle or a circle, for example, as shown in Figure 1, then we can take advantage of this by allowing the use of uniform finite difference grids or finite element meshes and hence of fast solvers for the numerical solution of the finite dimensional systems approximating (1.1) on such grids.

Fictitious domain methods can be traced back to the 1960's to Saulév [26]. The fictitious domain method, which was developed to handle problems with complex geometries in the stationary case [2, 16], has been recently applied to the case of the time dependent Maxwell's equations [7, 8, 9, 12]. In all these cases, a boundary Lagrange multiplier has been used to enforce the Dirichlet condition on the boundary of the obstacle. In [5] we compared our distributed multiplier approach to the boundary multiplier approach for the one-dimensional scalar wave equation and observed some advantages of our distributed multiplier formulation. We refer the reader to [5] for more details.

The advantage of our distributed multiplier method is that the problem in the fictitious domain can be discretized on a uniform mesh, independent of the boundary of the original domain, thus avoiding the time consuming construction of a boundary fitted mesh as in the finite element method. (However, there are some classes of fictitious domain methods that use boundary fitted meshes to improve accuracy [19].) At the same time, such an approach

is more accurate than the staircase approximation of the finite difference method. Thus, the distributed multiplier approach to Maxwell's equations presented in this paper provides a simple and much more accurate alternative to the popular FDTD method for the solution of Maxwell's equations. As will be shown here the approximation of the distributed multiplier approach is far superior to the staircase approximation of the FDTD method. In addition we also demonstrate the ease of implementing our fictitious domain method and provide details of the overhead costs which are minimal.

We consider a time-dependent problem of scattering by the obstacle  $\omega$ . We are interested in calculating the field in the exterior of  $\omega \subset \mathbb{R}^d$  with  $d = 2$  or  $d = 3$ . We do so by considering Maxwell's equations in free space with a Dirichlet boundary condition on  $\partial\omega$ , also known as a perfectly conducting condition (PEC). The evolution problem is to find  $\mathbf{E}$  and  $\mathbf{H}$  such that

$$\left( \begin{array}{l} \text{(i)} \quad \mu_0 \frac{\partial \mathbf{H}}{\partial t} + \nabla \times \mathbf{E} = 0, \quad \text{in } \mathbb{R}^d \setminus \bar{\omega} \times (0, T), \\ \text{(ii)} \quad \epsilon_0 \frac{\partial \mathbf{E}}{\partial t} - \nabla \times \mathbf{H} = 0, \quad \text{in } \mathbb{R}^d \setminus \bar{\omega} \times (0, T), \\ \text{(iii)} \quad \mathbf{E} \times \mathbf{n} = 0, \quad \text{on } \partial\omega \times (0, T), \\ \text{(iv)} \quad \mathbf{E}(\mathbf{x}, t = 0) = \mathbf{E}_0(\mathbf{x}), \quad \text{and } \mathbf{H}(\mathbf{x}, t = 0) = \mathbf{H}_0(\mathbf{x}), \quad \text{in } \mathbb{R}^d \setminus \bar{\omega}. \end{array} \right. \quad (1.3)$$

In (1.3),  $\mathbf{E}$ , and  $\mathbf{H}$  denote the electric and magnetic fields, respectively. The constants  $\epsilon_0$ , and  $\mu_0$  denote the permittivity and permeability of free space, respectively. The speed of light  $c$  is given to be  $c = 1/\sqrt{\epsilon_0\mu_0}$ . Also,  $\mathbf{n}$  is the unit outward normal vector to the boundary. The initial conditions  $\mathbf{E}_0$  and  $\mathbf{H}_0$  are known and assumed to be sufficiently smooth. This is an unbounded problem. One of the ways of simulating the scattering problem in an unbounded domain is to impose an absorbing boundary condition on the boundary of the truncated domain  $\Omega$  enclosing the obstacle  $\omega$ . Hence, we consider a finite domain  $\Omega$ , and we impose a first order (Silver-Müller) absorbing boundary condition on the (artificial) boundary  $\Gamma = \partial\Omega$ . Thus, our time dependent problem is now stated as an evolution problem to find  $\mathbf{E}$  and  $\mathbf{H}$  such that

$$\left( \begin{array}{l} \text{(i)} \quad \mu_0 \frac{\partial \mathbf{H}}{\partial t} + \nabla \times \mathbf{E} = 0, \quad \text{in } \Omega \setminus \bar{\omega} \times (0, T), \\ \text{(ii)} \quad \epsilon_0 \frac{\partial \mathbf{E}}{\partial t} - \nabla \times \mathbf{H} = 0, \quad \text{in } \Omega \setminus \bar{\omega} \times (0, T), \\ \text{(iii)} \quad \mathbf{E} \times \mathbf{n} = 0, \quad \text{on } \partial\omega \times (0, T), \\ \text{(iv)} \quad \mathbf{H} \times \mathbf{n} = \sqrt{\frac{\epsilon_0}{\mu_0}} \mathbf{n} \times (\mathbf{E} \times \mathbf{n}), \quad \text{on } \Gamma \times (0, T), \\ \text{(v)} \quad \mathbf{E}(\mathbf{x}, t = 0) = \mathbf{E}_0(\mathbf{x}), \quad \text{and } \mathbf{H}(\mathbf{x}, t = 0) = \mathbf{H}_0(\mathbf{x}), \quad \text{in } \Omega \setminus \bar{\omega}. \end{array} \right. \quad (1.4)$$

We will also consider a more accurate technique called a *perfectly matched layer* method to simulate such unbounded wave propagation problems in Section 7. The first order Silver-

Müller boundary conditions on  $\Gamma$  model the electromagnetic interactions between the domain  $\Omega$  and the exterior. They approximate the boundary  $\Gamma$  by its tangent plane. The outgoing electromagnetic plane waves which propagate normally to the boundary  $\Gamma$  of the domain  $\Omega$  can leave freely without being reflected at the boundary and are absorbed at the boundary. The Silver-Müller condition on  $\Gamma \times (0, T)$  is equivalent to the Sommerfeld radiation field condition for the Cartesian field components. Applying the Silver-Müller conditions at a finite distance from a spherical scatterer results in an approximate absorbing boundary condition which is exact for outgoing spherical waves [22].

An outline of the paper is as follows. In Section 2 we present a distributed Lagrange multiplier formulation for the problem (1.4). In Section 3 we present wellposedness results for our fictitious domain formulation using energy methods. In Section 4 we present a mixed finite element formulation for the (spatial) discretization of the fictitious domain problem and we present an iterative method for its solution in Section 5. Decay of discrete energies to obtain stability results are proved in Section 6. In Section 7 we replace the first order absorbing boundary condition by perfectly matched layers surrounding the computational domain. Numerical experiments are presented to validate our methods in Section 8 and we conclude with an outline of future work in Section 9.

## 2 A Fictitious Domain Method for Maxwell's Equations

In  $\mathbb{R}^3$ , let  $\mathbf{x} = (x, y, z)$ . We assume that neither the electromagnetic field excitation nor the modeled geometry has any variation in the  $z$ -direction. That is, we assume that all partial derivatives of the fields with respect to  $z$  equal zero, and the structure being modeled extends to infinity in the  $z$  direction with no change in the shape or position of its transverse cross section. In this case the six curl equations (1.4,i, ii) can be decoupled into two sets of equations each involving three electromagnetic field vectors. Let  $\mathbf{E} = (E_x, E_y, E_z)^T$ , and  $\mathbf{H} = (H_x, H_y, H_z)^T$  be the components of the electric and magnetic field vectors, respectively, in a Cartesian coordinate system. In the TE *mode* the electromagnetic field has three components  $H_z$ ,  $E_x$  and  $E_y$ . In the TM *mode* the electromagnetic field has the three components  $E_z$ ,  $H_x$  and  $H_y$ . The TE and TM modes are decoupled since they do not contain any common field vector components. These two modes are completely independent for structures that are composed of isotropic materials or anisotropic materials in which the off diagonal components in the constitutive tensors are absent [27].

We will consider the two-dimensional TM mode of Maxwell's equations. Let  $\Omega$  now be a bounded domain of  $\mathbb{R}^2$ , with  $\mathbf{x} = (x, y)^T$ . Let  $\mathbf{H} = (H_x, H_y)^T$  and let  $E = E_z$ . Let

$\mathbf{n} = (n_x, n_y)^T$  be the unit normal vector, and let us define the unit vector  $\mathbf{t} = (n_y, -n_x)^T$  pointing in the tangential direction. Then system (1.4) becomes

$$\left\{ \begin{array}{l} \text{(i)} \quad \mu_0 \frac{\partial \mathbf{H}}{\partial t} + \overrightarrow{\text{curl}} E = 0, \quad \text{in } \Omega \setminus \bar{\omega} \times (0, T), \\ \text{(ii)} \quad \epsilon_0 \frac{\partial E}{\partial t} - \text{curl } \mathbf{H} = 0, \quad \text{in } \Omega \setminus \bar{\omega} \times (0, T), \\ \text{(iii)} \quad E = 0, \quad \text{on } \partial\omega \times (0, T), \\ \text{(iv)} \quad \mathbf{H} \cdot \mathbf{t} = \sqrt{\frac{\epsilon_0}{\mu_0}} E, \quad \text{on } \Gamma \times (0, T), \\ \text{(v)} \quad E(\mathbf{x}, t = 0) = E_0(\mathbf{x}), \quad \text{and } \mathbf{H}(\mathbf{x}, t = 0) = \mathbf{H}_0(\mathbf{x}), \quad \text{in } \Omega \setminus \bar{\omega}. \end{array} \right. \quad (2.1)$$

In the above, the operator denoted by  $\overrightarrow{\text{curl}}$ , is a linear differential operator, which is defined as

$$\overrightarrow{\text{curl}} v = \left( \frac{\partial v}{\partial y}, -\frac{\partial v}{\partial x} \right) \quad \forall v \in \mathcal{D}'(\Omega), \quad (2.2)$$

where,  $\mathcal{D}'(\Omega)$  is the space of distributions on  $\Omega$ . Similarly, the linear differential operator denoted by  $\text{curl}$  is defined as

$$\text{curl } \mathbf{v} = \frac{\partial v_y}{\partial x} - \frac{\partial v_x}{\partial y} \quad \forall \mathbf{v} = (v_x, v_y) \in \mathcal{D}'(\Omega)^2. \quad (2.3)$$

The operator  $\text{curl}$  appears as the (formal) transpose of the operator  $\overrightarrow{\text{curl}}$  [10], i.e.,

$$\langle \text{curl } \mathbf{v}, \phi \rangle = \langle \mathbf{v}, \overrightarrow{\text{curl}} \phi \rangle, \quad \forall \mathbf{v} \in \mathcal{D}'(\Omega)^2, \phi \in \mathcal{D}'(\Omega). \quad (2.4)$$

In the case of the two dimensional TM mode, the PEC condition  $\mathbf{E} \times \mathbf{n} = 0$ , on  $\partial\omega \times (0, T)$  translates to

$$E = E_z = 0, \quad \text{on } \partial\omega \times (0, T). \quad (2.5)$$

We assume that the fields  $(E, \mathbf{H})$  are sufficiently differentiable in time. We note that (2.1,iv) is the Silver-Müller condition (1.4,iv) for the TM mode. The cross product  $\mathbf{H} \times \mathbf{n}$  can be written as  $\mathbf{H} \cdot \mathbf{t} \hat{z}$ , where  $\hat{z}$  is a unit vector in the  $z$  direction.

We employ the fictitious domain method introduced in [5] to enforce the Dirichlet boundary condition (2.1,iii) on the boundary  $\partial\omega$  of the obstacle  $\omega$ . The Silver-Müller boundary condition is naturally incorporated into the weak formulation that we construct by integrating (by parts) the equations (2.1,i, ii) over the domain  $\Omega$ , in (2.1,ii). Thus, the Silver-Müller boundary condition does not have to be enforced in the functional spaces. Using a distributed Lagrange multiplier approach problem (2.1) is equivalent, at least formally, to the variational problem

Find  $\{\tilde{E}(\cdot, t), \tilde{\mathbf{H}}(\cdot, t), \lambda(\cdot, t)\} \in H^1(\Omega) \times [L^2(\Omega)]^2 \times L^2(\omega)$  such that

$$\left( \begin{array}{l} \text{(i)} \quad \mu_0 \frac{d}{dt} \int_{\Omega} \tilde{\mathbf{H}} \cdot \boldsymbol{\Psi} \, d\mathbf{x} + \int_{\Omega} \overrightarrow{\text{curl}} \tilde{E} \cdot \boldsymbol{\Psi} \, d\mathbf{x} = 0, \quad \forall \boldsymbol{\Psi} \in [L^2(\Omega)]^2, \\ \text{(ii)} \quad \epsilon_0 \frac{d}{dt} \int_{\Omega} \tilde{E} \phi \, d\mathbf{x} - \int_{\Omega} \tilde{\mathbf{H}} \cdot \overrightarrow{\text{curl}} \phi \, d\mathbf{x} + \sqrt{\frac{\epsilon_0}{\mu_0}} \int_{\Gamma} \tilde{E} \phi \, d\Gamma, \\ \quad + \int_{\omega} \lambda \phi \, d\omega = 0, \quad \forall \phi \in H^1(\Omega), \\ \text{(iii)} \quad \int_{\omega} \tilde{E} \tau \, d\omega = 0, \quad \forall \tau \in L^2(\omega), \\ \text{(iv)} \quad \tilde{E}(\mathbf{x}, t=0) = \tilde{E}_0(\mathbf{x}), \quad \text{and} \quad \tilde{\mathbf{H}}(\mathbf{x}, t=0) = \tilde{\mathbf{H}}_0(\mathbf{x}), \quad \text{in } \Omega, \end{array} \right. \quad (2.6)$$

in the sense that

$$\tilde{E} = \begin{cases} E & \text{on } \Omega \setminus \bar{\omega}, \\ 0 & \text{on } \partial\omega. \end{cases}; \quad \tilde{\mathbf{H}} = \begin{cases} \mathbf{H} & \text{on } \Omega \setminus \bar{\omega}, \\ 0 & \text{on } \partial\omega. \end{cases} \quad (2.7)$$

The function  $\tilde{E}_0$  is chosen to be an  $H^1$ -extension of  $E_0$ , and  $\tilde{\mathbf{H}}_0$  to be at least an  $L^2$ -extension of  $\mathbf{H}_0$ . Thus, we have

$$\tilde{E}(\mathbf{x}, t=0) = \begin{cases} E_0(\mathbf{x}) & \text{on } \Omega \setminus \bar{\omega}, \\ 0 & \text{on } \omega. \end{cases}, \quad \tilde{\mathbf{H}}(\mathbf{x}, t=0) = \begin{cases} \mathbf{H}_0(\mathbf{x}) & \text{on } \Omega \setminus \bar{\omega}, \\ 0 & \text{on } \omega. \end{cases} \quad (2.8)$$

We note that, for  $E \in L^2(\Omega)$ ,  $\overrightarrow{\text{curl}} E = (\frac{\partial E}{\partial y}, -\frac{\partial E}{\partial x}) \in [L^2(\Omega)]^2$ , implies that both the partial derivatives of  $E$  must be in  $L^2(\Omega)$ . Hence we must have  $E \in H^1(\Omega)$ . In succeeding sections we will, however, drop the  $\tilde{\phantom{x}}$  symbol on the fields  $E$  and  $\mathbf{H}$ . Thus, the system (2.6) will read:

Find  $\{E(\cdot, t), \mathbf{H}(\cdot, t), \lambda(\cdot, t)\} \in H^1(\Omega) \times [L^2(\Omega)]^2 \times L^2(\omega)$  such that

$$\left( \begin{array}{l} \text{(i)} \quad \mu_0 \frac{d}{dt} \int_{\Omega} \mathbf{H} \cdot \boldsymbol{\Psi} \, d\mathbf{x} + \int_{\Omega} \overrightarrow{\text{curl}} E \cdot \boldsymbol{\Psi} \, d\mathbf{x} = 0, \quad \forall \boldsymbol{\Psi} \in [L^2(\Omega)]^2, \\ \text{(ii)} \quad \epsilon_0 \frac{d}{dt} \int_{\Omega} E \phi \, d\mathbf{x} - \int_{\Omega} \mathbf{H} \cdot \overrightarrow{\text{curl}} \phi \, d\mathbf{x} + \sqrt{\frac{\epsilon_0}{\mu_0}} \int_{\Gamma} E \phi \, d\Gamma, \\ \quad + \int_{\omega} \lambda \phi \, d\omega = 0, \quad \forall \phi \in H^1(\Omega), \\ \text{(iii)} \quad \int_{\omega} E \tau \, d\omega = 0, \quad \forall \tau \in L^2(\omega), \\ \text{(iv)} \quad E(\mathbf{x}, t=0) = E_0(\mathbf{x}), \quad \text{and} \quad \mathbf{H}(\mathbf{x}, t=0) = \mathbf{H}_0(\mathbf{x}) \quad \text{in } \Omega. \end{array} \right. \quad (2.9)$$

The idea behind the distributed fictitious domain method is to extend the electromagnetic solution inside the obstacle  $\omega$ , and solve Maxwell's equations in the entire domain  $\Omega$ . The Dirichlet condition on  $\partial\omega$  is enforced via the introduction of a Lagrange multiplier *on the entire domain*  $\omega$ . In [6, 12] a boundary multiplier fictitious domain method is introduced for the wave equation, and for Maxwell's equations.

### 3 Conservation of Energy

In this section we derive an energy identity from the variational formulation (2.9). The energy identity presented below guarantees the wellposedness of the problem, and the stability of the solution. Let  $(\cdot, \cdot)$  denote the  $L^2$  inner product in  $\Omega$ ,  $(\cdot, \cdot)_\omega$  the  $L^2$  inner product in  $\omega$ , and  $(\cdot, \cdot)_\Gamma$  the  $L^2$  inner product on  $\Gamma$ . Also, let  $\|\cdot\|, \|\cdot\|_\omega, \|\cdot\|_\Gamma$  denote the corresponding norms.

**Theorem 1** *The system (2.9) verifies the energy identity*

$$\frac{d}{dt} \mathcal{E} = -\sqrt{\frac{\epsilon_0}{\mu_0}} \|E\|_\Gamma^2, \quad (3.1)$$

where the energy  $\mathcal{E}$  is defined as

$$\mathcal{E} = \frac{1}{2} \{ \epsilon_0 \|E\|^2 + \mu_0 \|\mathbf{H}\|^2 \}, \quad (3.2)$$

with

$$\|\mu\|_\Gamma = \left( \int_\Gamma |\mu|^2 d\Gamma \right)^{1/2}. \quad (3.3)$$

Thus, (3.1) implies that the energy does not grow over time, i.e.,

$$\mathcal{E}(t) \leq \mathcal{E}(0), \quad \forall t > 0. \quad (3.4)$$

**Proof.** Let us take  $\phi = E$  in (2.9,ii). We obtain

$$\epsilon_0 \frac{d}{dt} \int_\Omega |E|^2 dx - \int_\Omega \mathbf{H} \cdot \overrightarrow{\text{curl}} E dx + \sqrt{\frac{\epsilon_0}{\mu_0}} \int_\Gamma |E|^2 d\Gamma + \int_\omega \lambda E d\omega = 0. \quad (3.5)$$

Next, we take  $\Psi = \mathbf{H}$  in (2.9,i). With this choice we get

$$\mu_0 \frac{d}{dt} \int_\Omega |\mathbf{H}|^2 dx + \int_\Omega \overrightarrow{\text{curl}} E \cdot \mathbf{H} dx = 0. \quad (3.6)$$

Adding equations (3.5) and (3.6) we have

$$\epsilon_0 \frac{d}{dt} \int_\Omega |E|^2 + \mu_0 \frac{d}{dt} \int_\Omega |\mathbf{H}|^2 dx + \sqrt{\frac{\epsilon_0}{\mu_0}} \int_\Gamma |E|^2 d\Gamma + \int_\omega \lambda E d\omega = 0, \quad (3.7)$$

which can be rewritten as

$$\frac{1}{2} \frac{d}{dt} (\epsilon_0 \|E\|^2 + \mu_0 \|\mathbf{H}\|^2) + \sqrt{\frac{\epsilon_0}{\mu_0}} \int_\Gamma |E|^2 d\Gamma + \int_\omega \lambda E d\omega = 0. \quad (3.8)$$

Taking  $\tau = \lambda$  in (2.9,iii) we obtain

$$\int_\omega E \lambda d\omega = 0. \quad (3.9)$$

Substituting (3.9) in (3.8), and using the definition of the energy (3.2) we obtain (3.1). ■

Equation (3.1) implies that there is no dissipation of the waves in the domain  $\Omega$ . This is the principle of *conservation of energy* for the variational formulation (2.9) for Maxwell's equation.

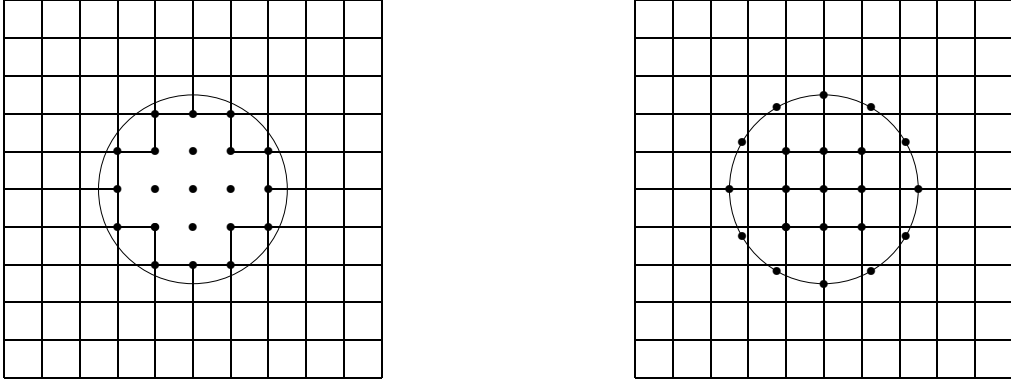


Figure 2: (left) A staircase approximation to a scattering disk. The disk is approximated by the highlighted nodal points. (right) The degrees of freedom,  $\Sigma_h^{\bar{\omega}}$ , for the Lagrange multiplier  $\lambda$  in the fictitious domain method, in the case of a scattering disk. The mesh ratio, i.e., the ratio of the step size chosen on the obstacle to the mesh step size, is about 1.3.

## 4 Numerical Discretization: A Mixed Finite Element Method

A very popular technique used to solve Maxwell's equations is the finite difference time domain method (FDTD) which uses a rectangular grid and an explicit scheme in time. The degrees of freedom of the electric and magnetic field are staggered in space and time. This method is computationally very efficient, however the staircase approximation to the obstacle is inaccurate, and it leads to excessive numerical diffraction when the obstacle boundary does not fit the mesh, as seen in Figure 2 (left). In this figure the scattering obstacle is a disk, and is approximated by the darkened nodal points. We now present details of the numerical approximation of problem (2.9)

### 4.1 Space Discretization

Let  $\Omega$  now be a union of rectangles such that we can consider a regular mesh ( $\mathcal{T}_h$ ) with square elements ( $K$ ) of edge length  $h > 0$  as in Figure 3. The approximation space for the electric field  $E$  is chosen to be

$$\mathcal{U}_h = \{\phi_h \in H^1(\Omega) \mid \forall K \in \mathcal{T}_h, \phi_h|_K \in Q_1\}, \quad (4.1)$$

where, the space  $Q_1 = P_{11}$ . The basis functions for  $E$  have unity value at one node and are zero at all other nodes. Figure 3 shows the locations for the degrees of freedom for both approximation spaces.

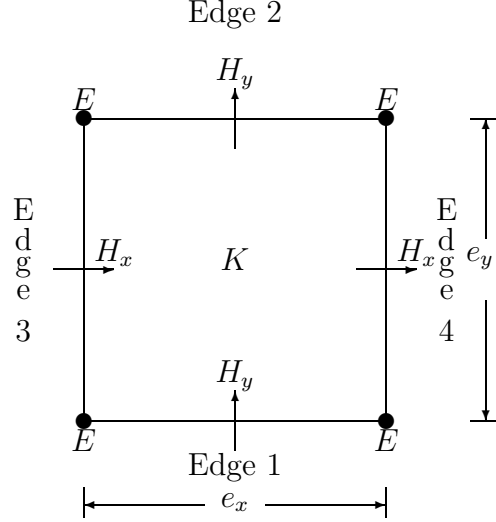


Figure 3: A sample domain element  $K$ . The degrees of freedom for the electric and magnetic field are staggered in space. The degrees of freedom for the electric field  $E$  are at the nodes of the square. The degrees of freedom for  $H_x$  and  $H_y$  are the midpoints of edges parallel to the  $x$ -axis and  $y$ -axis, respectively.

For the approximation of the magnetic field  $\mathbf{H}$  we need to consider a space  $\mathcal{V}_h$  that satisfies the property

$$\nabla \times \mathcal{U}_h \subset \mathcal{V}_h \quad (4.2)$$

in order to ensure a well posed formulation, see [20, 21, 17] for sufficient conditions for convergence of mixed methods. To this end we choose

$$\mathcal{V}_h = \{\Psi_h \in [L^2\Omega]^2 \mid \forall K \in \mathcal{T}_h, \Psi_h|_K \in RT_{[0]}\}, \quad (4.3)$$

where,  $RT_{[0]} = P_{10} \times P_{01}$ , is the lowest order Raviart Thomas space [24] and for  $k_1, k_2 \in \mathbb{N} \cup \{0\}$ ,

$$P_{k_1 k_2} = \{p(x_1, x_2) \mid p(x_1, x_2) = \sum_{0 \leq i \leq k_1} \sum_{0 \leq j \leq k_2} a_{ij} x_1^i x_2^j\}.$$

The basis functions for  $H_x$  and  $H_y$  have unity value along one  $e_y$  or  $e_x$  edge, respectively, and zero over all other edges (see Figure 3).

Let the set of mesh points on  $\bar{\Omega}$  be defined as

$$\Sigma_h = \{P \mid P \in \bar{\Omega}, P \text{ is a vertex of } \mathcal{T}_h\}. \quad (4.4)$$

Next, we define the set

$$\Sigma_h^{\bar{\omega}} = \{P \mid P \in \bar{\omega}, d(P, \partial\omega) \geq h\} \cup \text{Discrete set of points belonging to } \partial\omega. \quad (4.5)$$

The points on  $\partial\omega$  are typically chosen so that their distance is of the order of  $h$ . Using the sets defined above, we now define the set  $\mathbf{\Lambda}_h$  of the Lagrange multipliers by

$$\mathbf{\Lambda}_h = \{\mu_h \mid \mu_h = \sum_{P \in \Sigma_h^{\bar{\omega}}} \mu_P \chi_P, \mu_P \in \mathbb{R}\}, \quad (4.6)$$

with  $\chi_P$  the characteristic function of the elementary square of center  $P$  and edge length  $h$ ; we clearly have  $\mu_h(P) = \mu_P$ . We approximate the integrals involving the distributed multiplier by

$$\int_{\omega} \mu_h v_h \, dx \approx h^2 \sum_{P \in \Sigma_h^{\bar{\omega}}} \mu_h(P) v_h(P), \quad \forall v_h \in \mathbf{V}_h, \quad \forall \mu_h \in \mathbf{\Lambda}_h. \quad (4.7)$$

Figure 2 illustrates a choice for the set  $\Sigma_h^{\bar{\omega}}$  in the case of a scattering disk. The ratio of the distance between points on the circle, denoted by  $h_{\partial\omega}$ , to the mesh step size,  $h$ , is about 1.3. We will call this ratio as the *mesh ratio*. In numerical experiments, good results are observed when the mesh ratio is approximately 1.5 or greater [14]. Based on these approximation spaces, the space discrete scheme is defined as:

Find  $\{E_h(\cdot, t), \mathbf{H}_h(\cdot, t), \lambda_h(\cdot, t)\} \in \mathcal{U}_h \times \mathcal{V}_h \times \mathbf{\Lambda}_h$  such that

$$\left( \begin{array}{l} \text{(i)} \quad \mu_0 \frac{d}{dt} \int_{\Omega} \mathbf{H}_h \cdot \mathbf{\Psi}_h \, dx + \int_{\Omega} \overrightarrow{\text{curl}} E_h \cdot \mathbf{\Psi}_h \, dx = 0, \quad \forall \mathbf{\Psi}_h \in \mathcal{V}_h, \\ \text{(ii)} \quad \epsilon_0 \frac{d}{dt} \int_{\Omega} E_h \phi_h \, dx - \int_{\Omega} \mathbf{H}_h \cdot \overrightarrow{\text{curl}} \phi_h \, dx + \sqrt{\frac{\epsilon_0}{\mu_0}} \int_{\Gamma} E_h \phi_h \, d\Gamma, \\ \quad + \int_{\omega} \lambda_h \phi_h \, d\omega = 0, \quad \forall \phi_h \in \mathcal{U}_h, \\ \text{(iii)} \quad \int_{\omega} E_h \tau_h \, d\omega = 0, \quad \forall \tau_h \in \mathbf{\Lambda}_h, \\ \text{(iv)} \quad E_h(\mathbf{x}, t = 0) = E_{0,h}(\mathbf{x}), \quad \text{and} \quad \mathbf{H}_h(\mathbf{x}, t = 0) = \mathbf{H}_{0,h}(\mathbf{x}) \quad \text{in } \Omega. \end{array} \right. \quad (4.8)$$

## 4.2 Time Discretization

For the time discretization we use a centered second order accurate finite difference scheme in which the electric and magnetic field components are staggered in time,  $1/2$  units apart. For example, we compute the magnetic field at the time step  $n + 1/2$  and the electric field at the time step  $n + 1$ . On the interval  $[0, T]$ , let  $\Delta t = T/N$  be the time step, where  $N \in \mathbb{N}$ . We define  $V_h^k = V_h(t = k\Delta t)$  and denote  $t^k = k\Delta t$ , for  $k \in \mathbb{Z}$ . Following the notation in [3] we define for  $k \in \mathbb{Z}$

$$D_{\Delta t} V^k = \frac{V^{k+1/2} - V^{k-1/2}}{\Delta t}, \quad (4.9)$$

and

$$\bar{V}^k = \frac{V^{k+1/2} + V^{k-1/2}}{2}. \quad (4.10)$$

Using the notations and definitions developed above, the fully discrete scheme is given as

For  $n = 0, 1, \dots, N - 1$ , on the interval  $(t^n, t^{n+1})$ , given  $E_h^n, \mathbf{H}_h^{n-1/2}$

Find  $\{E_h^{n+1}, \mathbf{H}_h^{n+1/2}, \lambda_h^{n+1}\} \in \mathcal{U}_h \times \mathcal{V}_h \times \mathbf{\Lambda}_h$  such that

$$\left\{ \begin{array}{l} \text{(i)} \quad \mu_0(D_{\Delta t} \mathbf{H}_h^n, \Psi_h) + (\overrightarrow{\text{curl}} E_h^n, \Psi_h) = 0, \quad \forall \Psi_h \in \mathcal{V}_h, \\ \text{(ii)} \quad \epsilon_0(D_{\Delta t} E_h^{n+1/2}, \phi_h) - (\mathbf{H}_h^{n+1/2}, \overrightarrow{\text{curl}} \phi_h) + \sqrt{\frac{\epsilon_0}{\mu_0}} (\overline{E}_h^{n+1/2}, \phi_h)_\Gamma, \\ \quad \quad \quad + (\lambda_h^{n+1}, \phi_h)_\omega = 0, \quad \forall \phi_h \in \mathcal{U}_h, \\ \text{(iii)} \quad (E_h^{n+1}, \tau_h)_\omega = 0, \quad \forall \tau_h \in \mathbf{\Lambda}_h, \\ \text{(iv)} \quad E_h^0(\mathbf{x}) = E_{0,h}(\mathbf{x}), \quad \text{and} \quad \mathbf{H}_h^{-1/2}(\mathbf{x}) = \mathbf{H}_{0,h}(\mathbf{x}) - \frac{\Delta t}{2\mu_0} \overrightarrow{\text{curl}} E_{0,h}(\mathbf{x}) \quad \text{in } \Omega. \end{array} \right. \quad (4.11)$$

We will use quadrature rules for the calculation of all integrals involved in (4.8) due to which we obtain diagonal mass matrices and an explicit scheme in time. The use of quadrature formulas to obtain diagonal mass matrices is referred to as *mass-lumping*. Similarly, we use quadrature rules to calculate the boundary integrals as well. In this case system (4.11) in the absence of the distributed Lagrange multiplier, reduces to the FDTD scheme on a regular mesh.

## 5 Iterative Solution of the Discrete Problem

Let  $E_h^{\text{yee}}|^{n+1}$  be the electric field solution to (4.11) in the absence of the distributed multiplier (i.e., solution to the FDTD scheme). Then the update equations for the scheme (4.11) can be presented as follows. For an interior node  $(l, m)$  we have

$$\left\{ \begin{array}{l} \text{(i)} \quad H_x|_{l,m+1/2}^{n+1/2} = H_x|_{l,m+1/2}^{n-1/2} - \frac{\Delta t}{\mu_0 h} (E|_{l,m+1}^n - E|_{l,m}^n), \\ \text{(ii)} \quad H_y|_{l+1/2,m}^{n+1/2} = H_y|_{l+1/2,m}^{n-1/2} + \frac{\Delta t}{\mu_0 h} (E^n|_{l+1,m} - E^n|_{l,m}), \\ \text{(iii)} \quad E_h^{\text{yee}}|_{l,m}^{n+1} = E|_{l,m}^n + \frac{\Delta t}{\epsilon_0 h} (H_y|_{l+1/2,m}^{n+1/2} - H_y|_{l-1/2,m}^{n+1/2}) \\ \quad \quad \quad - \frac{\Delta t}{\epsilon_0 h} (H_x|_{l,m+1/2}^{n+1/2} - H_x|_{l,m-1/2}^{n+1/2}), \end{array} \right. \quad (5.1)$$

where for a solution component  $V_h^k$ ,  $V|_{l,m}^k = V_h^k(x = lh, y = mh)$ , with  $k, l, m \in \mathbb{Z}$ . For a node on the boundary  $\Gamma$ , the boundary integral

$$\int_\Gamma \overline{E}_h^{n+1/2} \phi_h d\Gamma, \quad (5.2)$$

will contribute terms to both the right hand side and the left hand side of equation (5.1,iii), as this term involves  $E_h^{n+1}$ , which is unknown, as well as  $E_h^n$ , which is known. In this case

(5.1,iii) has to be modified as

$$(iii) \quad E_h^{\text{yee}}|_{l,m}^{n+1} = \frac{\gamma^-}{\gamma^+} E|_{l,m}^n + \frac{\Delta t}{\epsilon_0 h \gamma^+} S \mathbf{H}|_{l,m}^{n+1/2}. \quad (5.3)$$

In the above

$$\gamma^- = \left( \frac{1}{\beta} - \frac{\kappa c \Delta t}{\alpha h} \right); \quad \gamma^+ = \left( \frac{1}{\beta} + \frac{\kappa c \Delta t}{\alpha h} \right), \quad (5.4)$$

where, for an interior node  $\beta = 1, \alpha = 1, \kappa = 0$ , for a boundary node but not a corner node  $\beta = 2, \alpha = 2, \kappa = 1$ , and for a boundary corner node  $\beta = 4, \alpha = 4, \kappa = 1$ . Also,  $S$  is the stiffness matrix associated with the integral

$$\int_{\Omega} \mathbf{H}_h^{n+1/2} \overrightarrow{\text{curl}} \phi_h \, d\mathbf{x}, \quad \forall \phi_h \in \mathcal{U}_h. \quad (5.5)$$

The solution  $E_h^{n+1}$  to the scheme (4.11) is obtained from the solution  $E_h^{\text{yee}}|^{n+1}$ , to the FDTD scheme (including absorbing boundary terms), by adjusting for the Dirichlet condition on the obstacle  $\omega$  via the Lagrange multiplier  $\lambda_h^{n+1}$ . Thus, we will solve a system of the form

Find  $(E_h^{n+1}, \lambda_h^{n+1}) \in \mathcal{U}_h \times \Lambda_h$  such that:

$$\begin{cases} D_h E_h^{n+1} + B_h^T \lambda_h^{n+1} = E_h^{\text{yee}}|^{n+1}, \\ B_h E_h^{n+1} = 0, \end{cases} \quad (5.6)$$

where  $D_h$  is the lumped mass matrix associated to the integral  $\int_{\Omega} E_h \phi_h \, d\mathbf{x}$ ,  $\forall \phi_h \in \mathcal{U}_h$ , and the matrix  $B_h$  is associated with with the integral (4.7). We note that  $D_h \in \mathbb{R}^{N \times N}$  is symmetric positive definite, and  $B_h \in \mathbb{R}^{M \times N}$  ( $M \ll N$ ). We use the *Schur Complement* of the system (5.6)

$$(B_h D_h^{-1} B_h^T) \lambda_h^{n+1} = B_h D_h^{-1} E_h^{\text{yee}}|^{n+1}, \quad (5.7)$$

to solve for  $\lambda_h^{n+1}$ . We do this by using an Uzawa-Type conjugate gradient algorithm in the form given in [15]. As remarked in [5], the matrix  $B_h D_h^{-1} B_h^T$  is symmetric and positive definite, a property that is related to a uniform discrete inf-sup condition associated with the integral (4.7). We refer the reader to [5, 14] for further details on inf-sup conditions for mixed problems.

## 6 Decay of Discrete Energies

In this section we prove a discrete energy identity based on the discretized fictitious domain formulation (4.11). This identity indicates the stability of the distributed multiplier formulation. An interesting fact to note is that the stability condition (CFL) is the same as in the

case of the problem without an obstacle. We define the bilinear form

$$a(\phi_h, \psi_h) = \int_{\Omega} \overrightarrow{\text{curl}} \phi_h \cdot \overrightarrow{\text{curl}} \psi_h \, dx, \forall (\phi_h, \psi_h) \in \mathcal{U}_h \times \mathcal{U}_h, \quad (6.1)$$

and the operator  $\mathcal{K}_h : \mathcal{U}_h \rightarrow \mathcal{U}'_h$  by

$$(\mathcal{K}_h \phi_h, \psi_h)_{\Omega} = a(\phi_h, \psi_h). \quad (6.2)$$

Let  $I$  be the identity operator on  $\mathcal{U}_h$ .

**Theorem 2** *If the CFL condition  $c\Delta t \leq h/\sqrt{2}$  is satisfied, then the operator*

$$\mathcal{S}_h = I - \frac{c^2 \Delta t^2}{4} \mathcal{K}_h, \quad (6.3)$$

*defines a positive quadratic form, the expression*

$$\mathcal{E}_h^{n+1} = \frac{1}{2} \left\{ \mu_0 \|\overline{\mathbf{H}}_h^{n+1}\|^2 + \epsilon_0 (E_h^{n+1}, \mathcal{S}_h E_h^{n+1}) \right\}, \quad (6.4)$$

*defines a discrete energy, and system (4.11) verifies the energy identity*

$$\mathcal{E}_h^{n+1} = \mathcal{E}_h^n - \Delta t \sqrt{\frac{\epsilon_0}{\mu_0}} \|\overline{E}_h^{n+1/2}\|_{\Gamma}^2, \quad \forall n \in \mathbb{N}, n \geq 0. \quad (6.5)$$

*Thus, (6.5) implies that the discrete energy does not grow over time, i.e.,*

$$\mathcal{E}_h^{n+1} \leq \mathcal{E}_h^n, \quad \forall n \geq 0. \quad (6.6)$$

**Proof.** We consider the mean value of (4.11,i) at  $n$  and  $n+1$ , with  $\Psi_h = \mathbf{H}_h^{n+1/2}$  to get

$$\mu_0 (\overline{D_{\Delta t} \mathbf{H}_h^{n+1/2}}, \mathbf{H}_h^{n+1/2}) + (\overrightarrow{\text{curl}} E_h^{n+1/2}, \mathbf{H}_h^{n+1/2}) = 0. \quad (6.7)$$

Using  $\phi_h = \overline{E}_h^{n+1/2}$  in (4.11,ii) we get

$$\epsilon_0 (D_{\Delta t} E_h^{n+1/2}, \overline{E}_h^{n+1/2}) - (\mathbf{H}_h^{n+1/2}, \overrightarrow{\text{curl}} \overline{E}_h^{n+1/2}) + \sqrt{\frac{\epsilon_0}{\mu_0}} \|\overline{E}_h^{n+1/2}\|_{\Gamma}^2 + (\lambda_h^{n+1}, \overline{E}_h^{n+1/2})_{\omega} = 0. \quad (6.8)$$

Taking the mean value of (4.11,iii) at  $n$  and  $n+1$  and by taking  $\mu_h = \lambda_h^{n+1}$ , we have

$$(\overline{E}_h^{n+1/2}, \lambda_h^{n+1})_{\omega} = 0. \quad (6.9)$$

Adding (6.7), (6.8), and (6.9) we get

$$\mu_0 (\overline{D_{\Delta t} \mathbf{H}_h^{n+1/2}}, \mathbf{H}_h^{n+1/2}) + \epsilon_0 (D_{\Delta t} E_h^{n+1/2}, \overline{E}_h^{n+1/2}) = -\sqrt{\frac{\epsilon_0}{\mu_0}} \|\overline{E}_h^{n+1/2}\|_{\Gamma}^2. \quad (6.10)$$

This implies

$$\begin{aligned} & \frac{1}{2\Delta t} \left\{ \mu_0(\mathbf{H}_h^{n+3/2}, \mathbf{H}_h^{n+1/2}) + \epsilon_0 \|E_h^{n+1}\|^2 \right\} \\ &= \frac{1}{2\Delta t} \left\{ \mu_0(\mathbf{H}_h^{n+1/2}, \mathbf{H}_h^{n-1/2}) + \epsilon_0 \|E_h^n\|^2 \right\} - \sqrt{\frac{\epsilon_0}{\mu_0}} \|\overline{E}_h^{n+1/2}\|_{\Gamma}^2. \end{aligned} \quad (6.11)$$

Using the parallelogram law we can write

$$\begin{aligned} (\mathbf{H}_h^{n+3/2}, \mathbf{H}_h^{n+1/2}) &= \frac{1}{4} \|\mathbf{H}_h^{n+3/2} + \mathbf{H}_h^{n+1/2}\|^2 - \frac{1}{4} \|\mathbf{H}_h^{n+3/2} - \mathbf{H}_h^{n+1/2}\|^2 \\ &= \|\overline{\mathbf{H}}_h^{n+1}\|^2 - \frac{\Delta t^2}{4} \|D_{\Delta t} \mathbf{H}_h^{n+1}\|^2. \end{aligned} \quad (6.12)$$

Similarly,

$$\begin{aligned} (\mathbf{H}_h^{n+1/2}, \mathbf{H}_h^{n-1/2}) &= \frac{1}{4} \|\mathbf{H}_h^{n+1/2} + \mathbf{H}_h^{n-1/2}\|^2 - \frac{1}{4} \|\mathbf{H}_h^{n+1/2} - \mathbf{H}_h^{n-1/2}\|^2 \\ &= \|\overline{\mathbf{H}}_h^n\|^2 - \frac{\Delta t^2}{4} \|D_{\Delta t} \mathbf{H}_h^n\|^2. \end{aligned} \quad (6.13)$$

From (6.12) and (4.11,i) we have

$$\begin{aligned} & \frac{1}{2} \left\{ \mu_0(\mathbf{H}_h^{n+3/2}, \mathbf{H}_h^{n+1/2}) + \epsilon_0 \|E_h^{n+1}\|^2 \right\} \\ &= \frac{1}{2} \left\{ \mu_0 \|\overline{\mathbf{H}}_h^{n+1}\|^2 - \frac{\Delta t^2}{4\mu_0} \|\overrightarrow{\text{curl}} E_h^{n+1}\|^2 + \epsilon_0 \|E_h^{n+1}\|^2 \right\} \\ &= \frac{1}{2} \left\{ \mu_0 \|\overline{\mathbf{H}}_h^{n+1}\|^2 + \epsilon_0 (E_h^{n+1}, \mathcal{S}_h E_h^{n+1}) \right\} \\ &= \mathcal{E}_h^{n+1}. \end{aligned} \quad (6.14)$$

Similarly we can show that

$$\frac{1}{2} \left\{ \mu_0(\mathbf{H}_h^{n+1/2}, \mathbf{H}_h^{n-1/2}) + \epsilon_0 \|E_h^n\|^2 \right\} = \mathcal{E}_h^n. \quad (6.15)$$

Substituting (6.14) and (6.15) in (6.11) we obtain the energy identity (6.5) In two dimensions we have,

$$\sup_{\phi_h \in \mathbf{U}_h} \frac{h^2 (\mathcal{K}_h \phi_h, \phi_h)_{L^2(\Omega)}}{4(\phi_h, \phi_h)_{L^2(\Omega)}} < 2, \quad (6.16)$$

which along with the CFL condition implies that

$$(\phi_h, \mathcal{S}_h \phi_h)_{L^2(\Omega)} = (\phi_h, (I - \frac{c^2 \Delta t^2}{4} \mathcal{K}_h) \phi_h)_{L^2(\Omega)} > 0, \quad \forall \phi_h \in \mathbf{U}_h \setminus \{0\}. \quad (6.17)$$

Equation (6.17) implies that the operator  $\mathcal{S}_h$  is positive definite. Thus, the CFL condition assures the stability of the scheme (4.11). ■

## 7 Construction of Perfectly Matched Layers

We use a perfectly matched layer model that is derived in [4]. The construction of this model follows the derivation of Sacks *et al.* in [25]. We outline the salient features of this construction below. We begin with a form of Maxwell's equations suitable for general media which permit both electric and magnetic currents but do not contain unbalanced electric charges, given as

$$\left( \begin{array}{l} \frac{\partial \mathbf{B}}{\partial t} = -\nabla \times \mathbf{E} - \mathbf{J}_M ; \quad (\text{Faraday's Law}) \\ \frac{\partial \mathbf{D}}{\partial t} = \nabla \times \mathbf{H} - \mathbf{J}_E ; \quad (\text{Ampere's Law}) \\ \nabla \cdot \mathbf{B} = 0 ; \quad (\text{Gauss's Law for the magnetic field}) \\ \nabla \cdot \mathbf{D} = 0 ; \quad (\text{Gauss's Law for the electric field}) \end{array} \right. \quad (7.1)$$

Constitutive relations which relate the electric and magnetic fluxes ( $\mathbf{D}, \mathbf{B}$ ) and the electric and magnetic currents ( $\mathbf{J}_E, \mathbf{J}_M$ ) to the electric and magnetic fields ( $\mathbf{E}, \mathbf{H}$ ) are added to these equations to make the system fully determined and to describe the response of a material to the electromagnetic fields. In empty space, these constitutive relations are  $\mathbf{D} = \epsilon_0 \mathbf{E}$ , and  $\mathbf{B} = \mu_0 \mathbf{H}$ , and  $\mathbf{J}_E = \mathbf{J}_M = 0$ , where  $\epsilon_0$  and  $\mu_0$  are the permittivity and the permeability of free space. In general, there are different possible forms for these constitutive relationships. In a frequency domain formulation of Maxwell's equations, these can be converted to linear relationships between the dependent and independent quantities with frequency dependent coefficient parameters.

We will derive a PML model in the frequency domain and then obtain a PML model in the time domain by taking the inverse Fourier transforms of the frequency domain equations. To this end, we consider the time-harmonic form of Maxwell's equations (7.1) given by

$$\left( \begin{array}{l} i\omega \hat{\mathbf{B}} = -\nabla \times \hat{\mathbf{E}} - \hat{\mathbf{J}}_M, \\ i\omega \hat{\mathbf{D}} = \nabla \times \hat{\mathbf{H}} - \hat{\mathbf{J}}_E, \\ \nabla \cdot \hat{\mathbf{B}} = 0, \\ \nabla \cdot \hat{\mathbf{D}} = 0, \end{array} \right. \quad (7.2)$$

where for every field vector  $\mathbf{V}$ ,  $\hat{\mathbf{V}}$  denotes its Fourier transform, and we have the constitutive laws

$$\left( \begin{array}{l} \hat{\mathbf{B}} = [\mu] \hat{\mathbf{H}}, \\ \hat{\mathbf{D}} = [\epsilon] \hat{\mathbf{E}}, \\ \hat{\mathbf{J}}_M = [\sigma_M] \hat{\mathbf{H}}, \\ \hat{\mathbf{J}}_E = [\sigma_E] \hat{\mathbf{E}}. \end{array} \right. \quad (7.3)$$

Here, the square brackets indicate a tensor quantity. Note that when the density of electric and magnetic charge carriers in the medium is uniform throughout space, then  $\nabla \cdot \hat{\mathbf{J}}_E = 0$  and  $\nabla \cdot \hat{\mathbf{J}}_M = 0$ . We define the new tensors

$$\begin{cases} [\bar{\mu}] &= [\mu] + \frac{[\sigma_M]}{i\omega}, \\ [\bar{\epsilon}] &= [\epsilon] + \frac{[\sigma_E]}{i\omega}. \end{cases} \quad (7.4)$$

Using the definitions (7.4) we define two new constitutive laws that are equivalent to (7.3), given by

$$\begin{cases} \hat{\mathbf{B}}_{\text{new}} &= [\bar{\mu}]\hat{\mathbf{H}}, \\ \hat{\mathbf{D}}_{\text{new}} &= [\bar{\epsilon}]\hat{\mathbf{E}}. \end{cases} \quad (7.5)$$

Using (7.5) in (7.2), Maxwell's equations, in time-harmonic form, become

$$\begin{cases} i\omega\hat{\mathbf{B}}_{\text{new}} &= -\nabla \times \hat{\mathbf{E}}, \\ i\omega\hat{\mathbf{D}}_{\text{new}} &= \nabla \times \hat{\mathbf{H}}, \\ \nabla \cdot \hat{\mathbf{B}}_{\text{new}} &= 0, \\ \nabla \cdot \hat{\mathbf{D}}_{\text{new}} &= 0. \end{cases} \quad (7.6)$$

To apply the perfectly matched layer to electromagnetic computations, we surround the computational domain with layers of finite depth in which the outgoing waves are trapped and attenuated. These layers are backed with a conventional boundary condition, such as a perfect electric conductor (PEC). This truncation of the layer will lead to reflections generated at the PEC surface, which can propagate back through the layer to re-enter the computational region. In this case, the reflection coefficient  $R$ , is a function of the angle of incidence  $\theta$ , the depth of the PML  $\delta$ , as well as the specific form of the tensors  $[\bar{\epsilon}]$  and  $[\bar{\mu}]$ . As shown in [25], the constitutive laws for the PML region are

$$[\bar{\epsilon}] = \epsilon_0[S], \quad (7.7)$$

$$[\bar{\mu}] = \mu_0[S], \quad (7.8)$$

and the correct form of the tensor  $[S]$  which appears in the constitutive laws is the product

$$[S] = [S]_x[S]_y[S]_z, \quad (7.9)$$

in which component  $[S]_\alpha$  in the product in (7.9) is responsible for attenuation in the  $\alpha$  direction, for  $\alpha = x, y, z$ . All three of the component tensors in (7.9) are diagonal and have the forms

$$[S]_x = \begin{bmatrix} s_x^{-1} & 0 & 0 \\ 0 & s_x & 0 \\ 0 & 0 & s_x \end{bmatrix}; \quad [S]_y = \begin{bmatrix} s_y & 0 & 0 \\ 0 & s_y^{-1} & 0 \\ 0 & 0 & s_y \end{bmatrix}; \quad [S]_z = \begin{bmatrix} s_z & 0 & 0 \\ 0 & s_z & 0 \\ 0 & 0 & s_z^{-1} \end{bmatrix}. \quad (7.10)$$

The constitutive laws for the perfectly matched layer are now given to be

$$\begin{cases} \hat{\mathbf{B}}_{\text{new}} &= \mu_0[S]\hat{\mathbf{H}}, \\ \hat{\mathbf{D}}_{\text{new}} &= \epsilon_0[S]\hat{\mathbf{E}}. \end{cases} \quad (7.11)$$

The parameters  $s_x, s_y,$  and  $s_z$  in the PML layers are chosen in order for the attenuation of waves in the PML to be sufficient so that the waves striking the PEC surface are negligible in magnitude. Perfectly matched layers are then placed near each edge (face in 3D) of the computational domain where a non-reflecting condition is desired. This leads to overlapping PML regions in the corners of the domain. When designing PML's for implementation, it is important to choose the parameters  $s_\alpha$  so that the resulting frequency domain equations can be easily converted back into the time domain. The simplest of these which we employ here [13] is

$$s_\alpha = 1 + \frac{\sigma_\alpha}{i\omega\epsilon_0}, \quad \text{where } \sigma_\alpha \geq 0 \quad \alpha = x, y, z. \quad (7.12)$$

Gedney [13] suggests a conductivity profile

$$\sigma_\alpha(\alpha) = \frac{\sigma_{\max}|\alpha - \alpha_0|^m}{\delta^m}; \quad \alpha = x, y, z. \quad (7.13)$$

where  $\delta$  is the depth of the layer,  $\alpha = \alpha_0$  is the interface between the PML and the computational domain, and  $m$  is the order of the polynomial variation. Gedney remarks that values of  $m$  between 3 and 4 are believed to be optimal. For the conductivity profile (7.13), the PML parameters can be determined for given values of  $m, \delta,$  and the desired reflection coefficient at normal incidence  $R_0,$  as

$$\sigma_{\max} \approx \frac{(m+1)\ln(1/R_0)}{2\eta\delta}, \quad (7.14)$$

$\eta$  being the characteristic wave impedance of the PML. Empirical testing suggests that, for a broad range of problems, an optimal value of  $\sigma_{\max}$  is given by

$$\sigma_{\text{opt}} \approx \frac{m+1}{150\pi\Delta_\alpha\sqrt{\epsilon_r}}, \quad (7.15)$$

where  $\Delta_\alpha$  is the space increment in the  $\alpha$  direction and  $\epsilon_r$  is the relative permittivity of the material being modeled. In the case of free space  $\epsilon_r = 1.$

From the time-harmonic Maxwell's curl equations in the PML (7.6) and (7.11), Ampere's and Faraday's laws can be written in the most general form as

$$\begin{cases} i\omega\mu_0[S]\hat{\mathbf{H}} &= -\nabla \times \hat{\mathbf{E}} \quad ; \quad (\text{Faraday's Law}) \\ i\omega\epsilon_0[S]\hat{\mathbf{E}} &= \nabla \times \hat{\mathbf{H}} \quad ; \quad (\text{Ampere's Law}) \end{cases} \quad (7.16)$$

In the presence of the diagonal tensor  $[S]$ , a plane wave is purely transmitted into the PML.

To obtain the two dimensional model of the PML, we assume no variation in the  $z$  direction (i.e.,  $\frac{\partial}{\partial z} = 0$ ). In the two dimensional TM mode the electromagnetic field has three components,  $E_z, H_x$ , and  $H_y$ . In this case, we have  $\sigma_z = 0$  and  $s_z = 1$  in the PML and the time-harmonic Maxwell's equations (7.16), in the PML medium can be written in scalar form as:

$$\begin{cases} i\omega\mu_0 \frac{s_y}{s_x} \hat{H}_x &= -\frac{\partial \hat{E}_z}{\partial y}, \\ i\omega\mu_0 \frac{s_x}{s_y} \hat{H}_y &= -\frac{\partial \hat{E}_z}{\partial x}, \\ i\omega\epsilon_0 s_x s_y \hat{E}_z &= \frac{\partial \hat{H}_y}{\partial x} - \frac{\partial \hat{H}_x}{\partial y} \end{cases} \quad (7.17)$$

To avoid a computationally intensive implementation, we do not insert the expressions for  $s_x, s_y$  and  $s_z$ , obtained via (7.12), into (7.16), and transform to the time domain. Instead, we define suitable constitutive relationships that facilitate the decoupling of the frequency dependent terms [27]. To this end, we introduce the fields

$$\begin{cases} \hat{B}_x &= \mu_0 s_x^{-1} \hat{H}_x, \\ \hat{B}_y &= \mu_0 s_y^{-1} \hat{H}_y, \\ \hat{D}_z &= \mu_0 s_y \hat{E}_z. \end{cases} \quad (7.18)$$

Substituting the definitions (7.18) in (7.17), using the defining relations for  $s_x$  and  $s_y$  from (7.12), and then transforming into the time domain by using the inverse Fourier transform, yields an equivalent system of time-domain differential equations, which is the two dimensional TM mode of the PML given as

$$\begin{cases} \frac{\partial \mathbf{B}}{\partial t} &= -\frac{1}{\epsilon_0} \Sigma_2 \mathbf{B} - \overrightarrow{\text{curl}} E, \\ \frac{\partial \mathbf{H}}{\partial t} &= \frac{1}{\mu_0} \frac{\partial \mathbf{B}}{\partial t} + \frac{1}{\epsilon_0 \mu_0} \Sigma_1 \mathbf{B}, \\ \frac{\partial D}{\partial t} &= -\frac{1}{\epsilon_0} \sigma_x D + \text{curl } \mathbf{H}, \\ \frac{\partial E}{\partial t} &= -\frac{1}{\epsilon_0} \sigma_y E + \frac{1}{\epsilon_0} \frac{\partial D}{\partial t}, \end{cases} \quad (7.19)$$

with  $\mathbf{H} = (H_x, H_y)^T$ ,  $\mathbf{B} = (B_x, B_y)^T$ ,  $E = E_z$  and  $D = D_z$ . Also,

$$\Sigma_1 = \begin{pmatrix} \sigma_x & 0 \\ 0 & \sigma_y \end{pmatrix}; \quad \Sigma_2 = \begin{pmatrix} \sigma_y & 0 \\ 0 & \sigma_x \end{pmatrix}. \quad (7.20)$$

Thus, the PML model consists in solving system (7.19) for the six variables,  $B_x, B_y, H_x, H_y, D_z, E_z$ .

In order to use the PML model, instead of the first order Silver-Müller boundary condition, we replace the discrete model (5.1)-(5.3) by the PML model and then account for the Dirichlet condition on the boundary of the obstacle using (5.6). The distributed multiplier formulation with perfectly matched layers is then given to be

Find  $(E_h^{\text{yee}|n+1}, D_h^{n+1}, \mathbf{H}_h^{n+\frac{1}{2}}, \mathbf{B}_h^{n+\frac{1}{2}}) \in \mathcal{U}_h \times \mathcal{U}_h \times \mathcal{V}_h \times \mathcal{V}_h$  such that for all  $\Psi_h \in \mathcal{V}_h$ , for all  $\phi_h \in \mathcal{U}_h$ ,

$$\left( \begin{array}{l} \text{(i)} \\ \text{(ii)} \\ \text{(iii)} \\ \text{(iv)} \end{array} \right. \begin{array}{l} (D_{\Delta t} \mathbf{B}_h^n, \Psi_h) \\ (D_{\Delta t} \mathbf{H}_h^n, \Psi_h) \\ (D_{\Delta t} D_h^{n+\frac{1}{2}}, \phi_h) \\ (D_{\Delta t} E_h^{\text{yee}|n+\frac{1}{2}}, \phi_h) \end{array} = \begin{array}{l} -\frac{1}{\epsilon_0} (\Sigma_2 \overline{\mathbf{B}}_h^n, \Psi_h) \\ \frac{1}{\mu_0} (D_{\Delta t} \mathbf{B}_h^n, \Psi_h) \\ -\frac{1}{\epsilon_0} (\sigma_x \overline{D}_h^{n+\frac{1}{2}}, \phi_h) \\ -\frac{1}{\epsilon_0} (\sigma_y \overline{E}_h^{\text{yee}|n+\frac{1}{2}}, \phi_h) \end{array} - \begin{array}{l} (\overrightarrow{\text{curl}} E_h^n, \Psi_h), \\ \frac{1}{\epsilon_0 \mu_0} (\Sigma_1 \overline{\mathbf{B}}_h^n, \Psi_h), \\ (\overrightarrow{\text{curl}} \phi_h, \mathbf{H}_h^{n+\frac{1}{2}}), \\ \frac{1}{\epsilon_0} (D_{\Delta t} D_h^{n+\frac{1}{2}}, \phi_h). \end{array} \right. \quad (7.21)$$

In the above

$$D_{\Delta t} E_h^{\text{yee}|n+1/2} = \frac{E_h^{\text{yee}|n+1} - E_h^n}{\Delta t}, \quad (7.22)$$

and

$$\overline{E}_h^{\text{yee}|n+1/2} = \frac{E_h^{\text{yee}|n+1} + E_h^n}{2}. \quad (7.23)$$

Once we obtain the solution to the system (7.21), the solution to the scattering problem is obtained by solving system (5.6).

## 8 Numerical Examples: Scattering by a Disk

We consider the scattering of the harmonic planar waves  $e^{-i(\rho t - \mathbf{k} \cdot \mathbf{x})}$  by a perfectly reflecting disk whose radius is 0.25 m. The disc is located at the center of the domain  $[0, 3.5] \times [0, 3.5]$ . The frequency,  $f$ , is 0.6 GHz, and the wavelength,  $L$ , is 0.5 m. The angular frequency is  $\rho = 2\pi f$ . The wave illuminates  $\omega$  from the left and propagates horizontally. The distance from the disk to the absorbing boundary is 3 wavelengths. We have used a rectangular mesh consisting of  $113 \times 113$  nodes, with the mesh step size  $h = 0.5/16$  m. The time step is  $\Delta t = 2\pi/(25\rho)$ . Thus, the Courant number is  $(c\Delta t)/h = 0.64$ . We have also considered mesh refinements in order to estimate the accuracy of our solution.

In Figure 4 we plot the number of degrees of freedom (DOF) of the Lagrange multiplier on the boundary of the disk,  $\partial\omega$ , as a function of the mesh ratio,  $h_{\partial\omega}/h$ , for different discretizations, where  $h_{\partial\omega}$  is defined as the step size on the boundary of the disk. As can be seen from Figure 4, for fine meshes, as opposed to coarse meshes, bigger changes in the DOF on the boundary of the disk result from a small change in the mesh ratio. The Uzawa algorithm

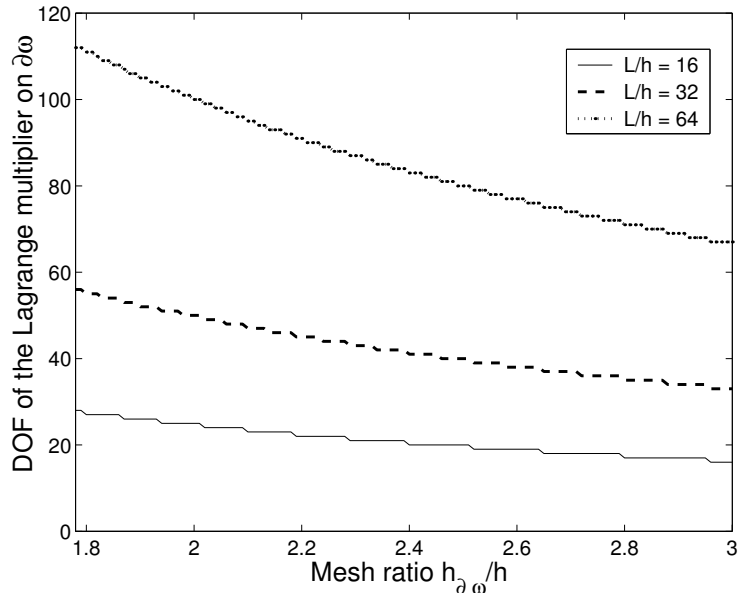


Figure 4: The number of degrees of freedom (DOF) of the Lagrange multiplier on the boundary of the disk versus the mesh ratio  $h_{\partial\omega}/h$ .

converges in a finite number of iterations for values of  $h_{\partial\omega}/h$  between 1.5 and 3. However, for certain values between 1.5 and 1.8 the behavior of the Uzawa algorithm is unstable with respect to number of iterations. Thus we consider values for  $h_{\partial\omega}/h$  between 1.8 and 3.

For this test problem the exact solution is known when  $\Gamma$  is located at infinity. In Figures 5, 6 and 7, we plot the error (point-wise difference) between each computed solution and the exact solution for discretizations with 16, 32 and 64 nodes per wavelength, respectively. It is clearly observed that, as the mesh is refined, the error in the fictitious domain method with the Silver-Müller condition is dominated by reflections from the artificial boundary. In the case of the PML model the error in the discretization of the Lagrange multiplier dominates the total error.

Next, we define the relative error (RE) between the exact solution and a computed solution as

$$\text{RE} = \frac{\|E_{\text{exact}} - E_C\|_{L^2(\Omega)}}{\|E_{\text{exact}}\|_{L^2(\Omega)}}, \quad (8.1)$$

where  $E_{\text{exact}}$  stands for the exact solution, and  $E_C$  denotes a computed solution. In Figure 8 we plot the relative error for the fictitious domain method with a PML of thickness  $L/4$ , against the mesh ratio  $h_{\partial\omega}/h$ , for different discretizations. From Figure 8 (left) we can see that the relative error can vary by a factor of 2 for different values of the mesh ratio. In this figure we also plot (right) ratios of relative errors between successive mesh refinements obtained from Figure 8 (left). The solid line represents the ratio of the relative error for a discretization with 16 nodes per wavelength, and the relative error of a discretization with

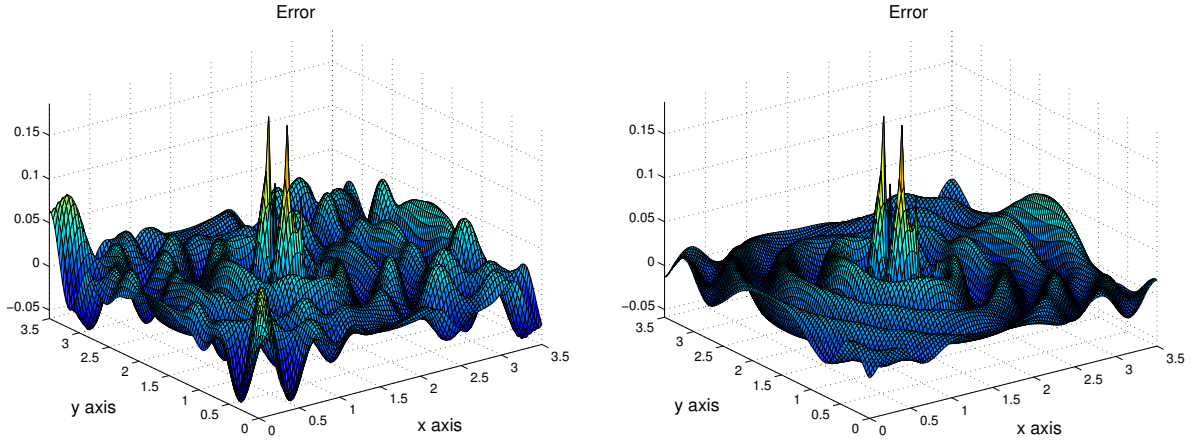


Figure 5: Plot of the error between the exact solution and the fictitious domain method for a discretization with 16 nodes per wavelength: (left) with the Silver-Müller boundary condition; (right) with a 4 cell PML.

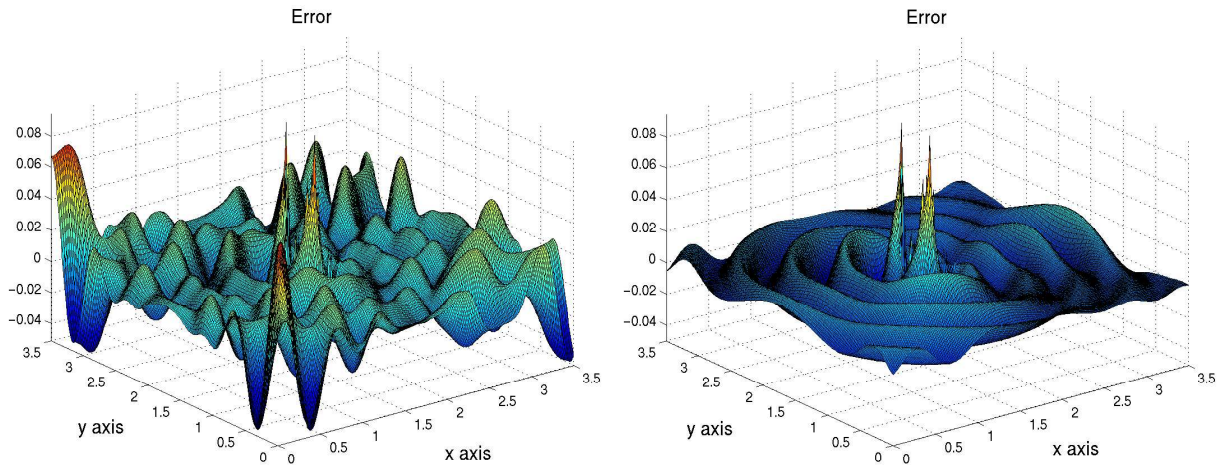


Figure 6: Plot of the error between the exact solution and the fictitious domain method for a discretization with 32 nodes per wavelength: (left) with the Silver-Müller boundary condition; (right) with a 4 cell PML.

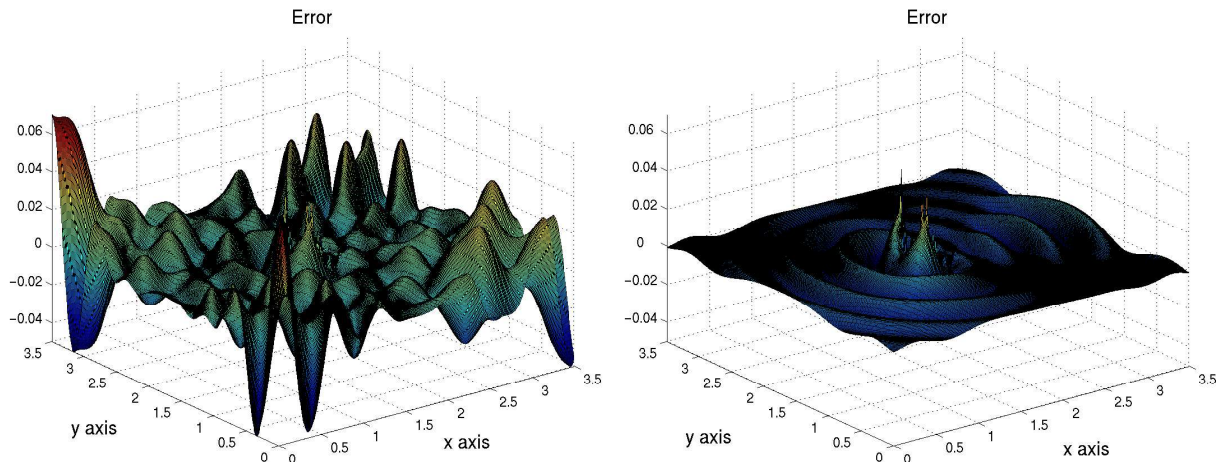


Figure 7: Plot of the error between the exact solution and the fictitious domain method for a discretization with 64 nodes per wavelength: (left) with the Silver-Müller boundary condition; (right) with a 4 cell PML.

32 nodes per wavelength. Similarly, the dashed line denotes the ratio of relative errors for discretizations with 32 and 64 nodes per wavelength. Again, we observe that the ratios can vary by almost a factor of 3.

In Figures 9 we plot the maximum and the minimum iteration counts, respectively, that are required for the convergence of the Uzawa algorithm, as a function of the mesh ratio. These results are for the fictitious domain method with a PML of thickness  $L/4$ . The number of iterations for the three discretizations is seen to be bounded by 20.

In Table 1 we present relative errors and maximum and minimum iteration counts for the fictitious domain method with PML's of thickness,  $L/4$ ,  $L/2$  and  $L$ . The relative error in all three cases is almost the same. Thus, we do not obtain any benefit by increasing the thickness of the PML as the dominating error is due to the discretization of the Lagrange multiplier. This can also be observed in the Figures 5, 6, and 7. A quarter wavelength thick PML is sufficient to obtain significant improvements over the first order boundary condition.

In Table 2 we present relative errors and maximum and minimum iteration counts for the fictitious domain method with the Silver-Müller boundary condition. As observed in Figures 5, 6, and 7, reflections from the artificial boundary dominate the error. Thus, we do not expect to see much improvement in the error as the mesh is refined. As seen in Table 1, the relative error for a discretization with 64 nodes per wavelength is 4 times smaller than the error for the same discretization with the Silver-Müller boundary condition.

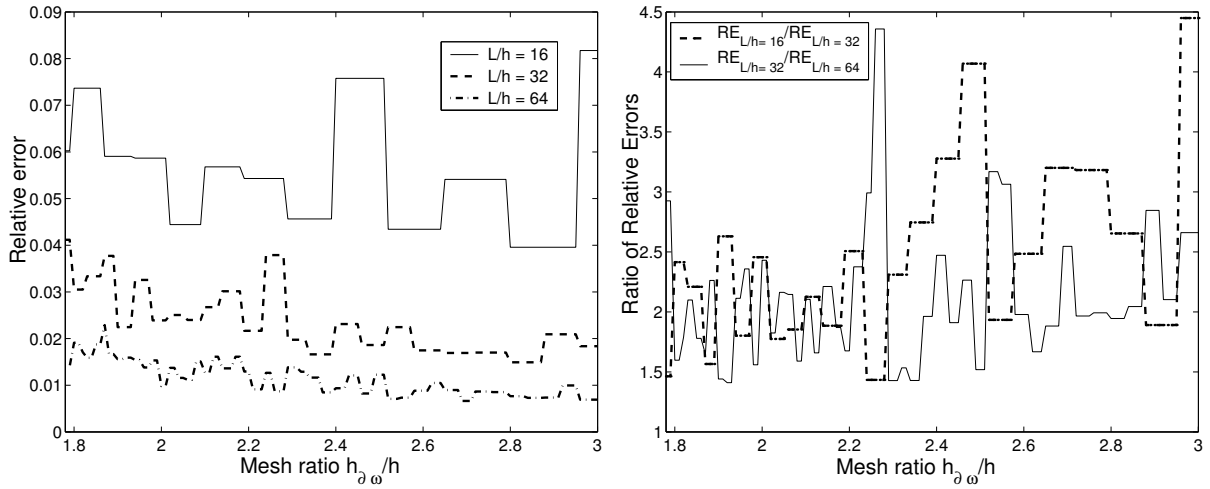


Figure 8: (left) Plot of the relative error versus the mesh ratio  $h_{\partial\omega}/h$  for three different discretizations. (right) Plot of ratios of successive relative errors versus the mesh ratio  $h_{\partial\omega}/h$ .

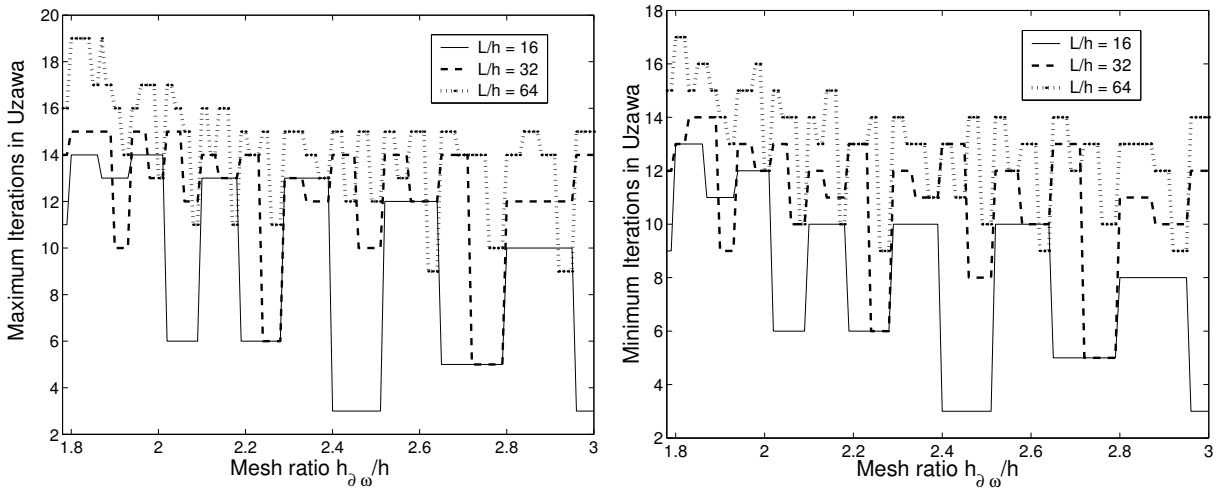


Figure 9: The maximum (left) and minimum (right) number of iterations required for the Uzawa algorithm versus the mesh ratio  $h_{\partial\omega}/h$  for three different discretizations.

PML	$h$	$\Delta t$	RE	Max Iter	Min Iter
$L/4$	$L/16$	$L/(25c)$	5.867e-2	14	12
	$L/32$	$L/(50c)$	2.389e-2	13	12
	$L/64$	$L/(100c)$	9.830e-3	13	12
$L/2$	$L/16$	$L/(25c)$	5.815e-2	14	12
	$L/32$	$L/(50c)$	2.389e-2	13	12
	$L/64$	$L/(100c)$	9.830e-3	13	12
$L$	$L/16$	$L/(25c)$	5.815e-2	14	12
	$L/32$	$L/(50c)$	2.389e-2	13	12
	$L/64$	$L/(100c)$	9.829e-3	13	12

Table 1: Table of relative errors of the fictitious domain solutions, for PML's of varying thickness, computed with respect to the exact solution.

$h$	$\Delta t$	SM		
		RE	Max Iter	Min Iter
$L/16$	$L/(25c)$	7.026e-2	14	12
$L/32$	$L/(50c)$	4.519e-2	13	12
$L/64$	$L/(100c)$	3.854e-2	13	12

Table 2: Table of relative errors of the fictitious domain solution, with the Silver-Müller (SM) boundary condition, computed with respect to the exact solution for different discretizations.

Finally, in Table 3, we present relative errors and maximum and minimum iteration counts for the fictitious domain method with a PML of thickness  $L/4$ , for different values of the mesh ratio  $h_{\partial\omega}/h$ , and for different discretizations. For a given discretization, the relative errors are comparable for different values of the mesh ratio. We observe that the ratios between successive relative errors, for a fixed value of the mesh ratio, is approximately 2. Thus, the spatial accuracy of the fictitious domain method, based on these results, seems to be about first order.

$h$	$\Delta t$	$h_{\partial\omega}/h$	PML ( $L/4$ )		
			RE	Max Iter	Min Iter
$L/16$	$L/(25c)$	2.0	5.867e-2	14	12
		2.4	7.577e-2	3	3
		2.7	5.412e-2	5	5
$L/32$	$L/(50c)$	2.0	2.389e-2	13	12
		2.4	2.312e-2	14	13
		2.7	1.691e-2	14	13
$L/64$	$L/(100c)$	2.0	9.830e-3	13	12
		2.4	9.355e-3	15	13
		2.7	6.641e-3	14	12
$L/128$	$L/(200c)$	2.0	6.972e-3	16	15
		2.4	4.957e-3	16	14
		2.7	4.679e-3	13	11

Table 3: Table of relative errors of the fictitious domain solutions for a PML of thickness  $L/4$ , computed with respect to the exact solution, for different values of the mesh ratio  $h_{\partial\omega}/h$  and different discretizations.

In Table 4 we compare the fictitious domain approach to a staircase approach using the finite difference time domain method. As can be seen from the table, the fictitious domain method provides a significant improvement over the staircase approximation. This is also evident from Figures 10 and 11, which compare the errors for both methods for 16 and 64 nodes per wavelength.

$N$	$L/h$	Staircase	Fictitious Domain
$113^2$	16	1.959e-1	5.867e-2
$225^2$	32	9.997e-2	2.389e-2
$449^2$	64	4.871e-2	9.830e-3
$897^2$	128	2.619e-2	6.972e-3

Table 4: Table of relative errors for the fictitious domain solution for a PML of thickness  $L/4$ , and relative errors for a staircase approximation for different nodes per wavelength.

So far we have presented results in which the frequency  $f$ , and hence the wavelength  $L$ , in the domain was fixed. As the frequency is increased, i.e., the wavelength is decreased, the effects of dispersion start to degrade the solution. The error in the solution is no longer dominated by the error in the discretization of the Lagrange multiplier. The error at higher frequencies is dominated by large phase errors, which accumulate over time and can significantly affect the solution. To study the errors that arise at high frequencies, we have

calculated the relative errors in the case when  $f = 1.2, 2.4$  and  $4.8$  GHz. The relative error is a combination of the error in the amplitude of the solution as well as the error in the phase. To see the dominance of the phase error, we also calculate a relative amplitude error and a phase error for each frequency. In these calculations the size of the domain is fixed. We use a fixed step size  $h = 0.5/128$ , which uses 128 nodes per wavelength at the lowest frequency of 0.6 GHz, on the square domain  $[0, 3.5] \times [0, 3.5]$ . Thus, we have  $897 \times 897$  nodes with  $N = 897$ . The time step is chosen so that the stability condition as before is  $\eta = 0.64$ . The results are all computed after 1400 iterations. All results are computed using a 4 cell PML and the fictitious domain method. We do not observe any significant reduction in the errors by increasing the thickness of the PML layer.

In Figure 12 we plot a top view of the solutions with  $f = 0.6$  GHz (top) and  $f = 1.2$  GHz (bottom). In Figure 13 we plot a top view of the solutions with  $f = 2.4$  GHz (top) and  $f = 4.8$  GHz (bottom). The computed solutions qualitatively compare well with the exact solution.

Let  $R_{\text{exact}}$  and  $I_{\text{exact}}$  denote the real and imaginary parts of the exact solution. Similarly, let  $R_C$  and  $I_C$  denote the real and imaginary parts of our computed solution. We define the phase error (PE) as

$$\text{PE}(x) = \tan^{-1} \left( \frac{I_{\text{exact}}(x)}{R_{\text{exact}}(x)} \right) - \tan^{-1} \left( \frac{I_C(x)}{R_C(x)} \right). \quad (8.2)$$

We also calculate the phase error in degrees per node as

$$\text{Phase error} = \frac{360}{2\pi N} \left( \sum_{k=1}^{N^2} |\text{PE}(x_k)|^2 \right)^{1/2} \text{ degrees/node}, \quad (8.3)$$

where  $x_k$  is a node of the finite element triangulation  $\mathcal{T}_h$ . The amplitude error (AE) is defined as

$$\text{AE}(x) = \sqrt{(I_{\text{exact}}(x))^2 + (R_{\text{exact}}(x))^2} - \sqrt{(I_C(x))^2 + (R_C(x))^2}. \quad (8.4)$$

Next, we calculate a relative amplitude error (RAE) for each frequency which will be the ratio of the  $L^2$  norm of the amplitude error to the  $L^2$  norm of the amplitude of the exact solution in the computational domain. In Figure 14 we plot linear gray scale images of the phase error (top) and the amplitude error (bottom) over the square domain. In this figure we can see that the phase error is the smallest along the grid diagonals and it is the largest along the axis of the mesh.

In Table 5 we present the (total) relative errors for the real and imaginary parts of the solution. As expected the relative errors increase as the frequency is increased. We also compare the relative amplitude error RAE which is calculated using the amplitude error AE

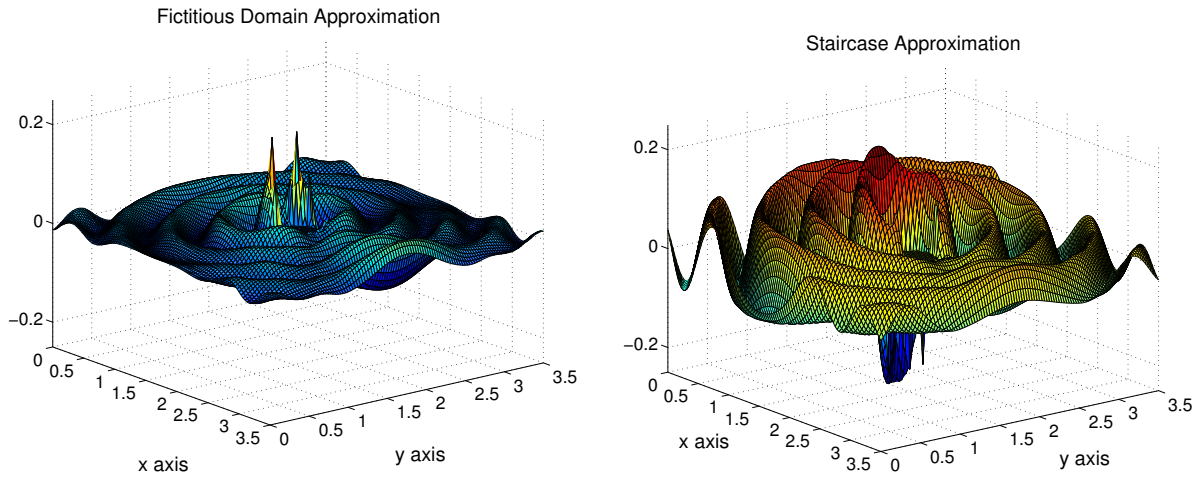


Figure 10: (left) Plot of the error between the exact solution and the fictitious domain method with a 4 cell PML. (right) Plot of the error between the exact solution and a staircase approximation. In both cases we use a discretization with 16 nodes per wavelength.

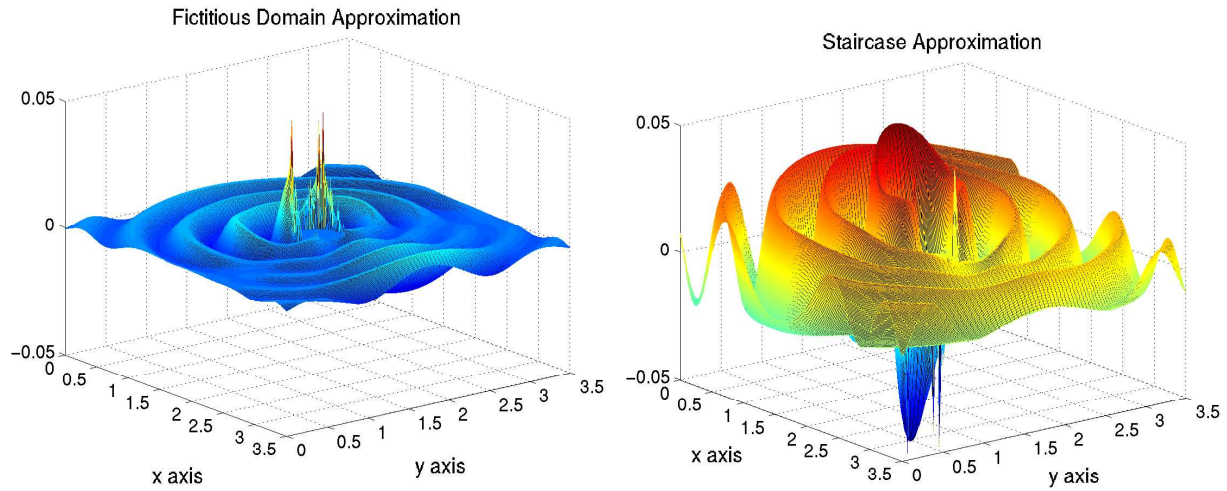


Figure 11: (left) Plot of the error between the exact solution and the fictitious domain method with a 4 cell PML. (right) Plot of the error between the exact solution and a staircase approximation. In both cases we use a discretization with 64 nodes per wavelength.

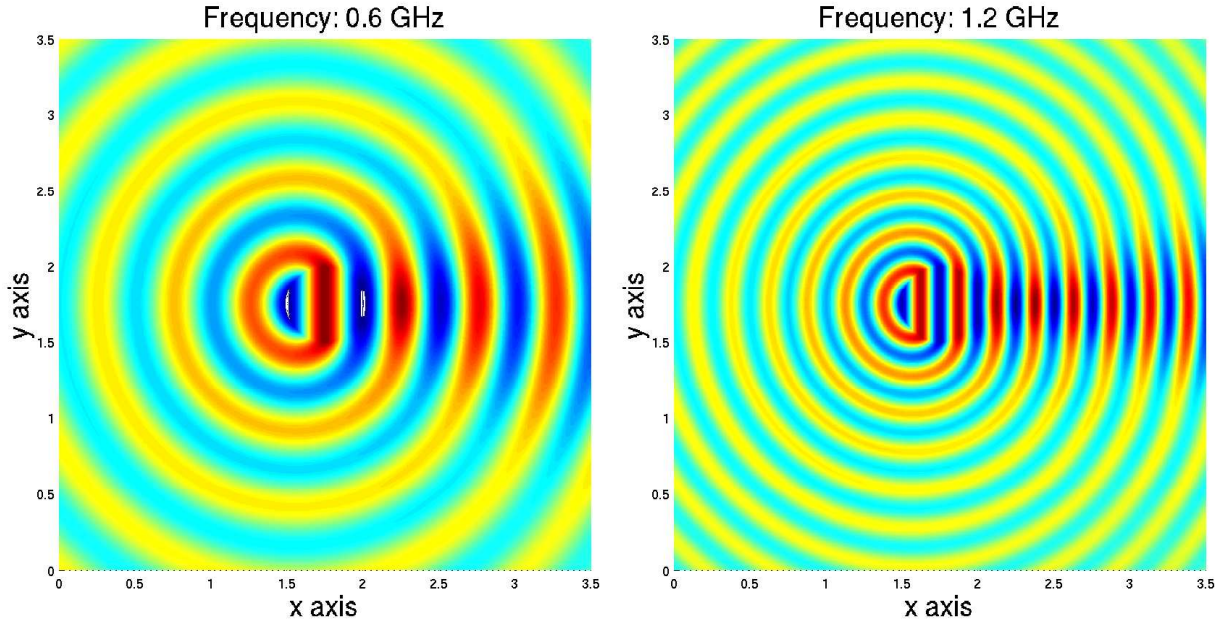


Figure 12: A top view of the computed solution (real part) for a harmonic planar wave with frequency  $f = 0.6$  GHz and  $L = 0.5$ m (left), and for a harmonic planar wave with frequency  $f = 1.2$  GHz and  $L = 0.25$ m (right).

defined in (8.4). Finally we compare the phase error in degrees per node, defined in (8.3), for each case. We observe that the relative amplitude error is significantly better than the total relative errors. As can be seen from the table the phase error increases significantly at higher frequencies. For  $f = 0.6$  GHz, the phase error is 0.37 degrees per node. This error increases to 15.69 degrees per node when  $f = 4.8$  GHz.

$f$ (GHz)	$L$ (m)	$L/h$	RE (Real)	RE (Imag)	RAE	Phase
0.6	0.5	128	6.97e-3	7.77e-3	3.31e-3	0.37
1.2	0.25	64	1.57e-2	1.52e-2	5.72e-3	0.73
2.4	0.125	32	4.97e-2	4.72e-2	1.11e-2	2.29
4.8	0.0625	16	2.89e-1	2.93e-1	2.57e-2	15.69

Table 5: Table of errors for the fictitious domain solution for a PML of thickness  $L/4$ , at different frequencies. The relative error for the real and imaginary parts of the solution is given. RAE is a relative amplitude error and the phase error in degrees per node in each case is provided.

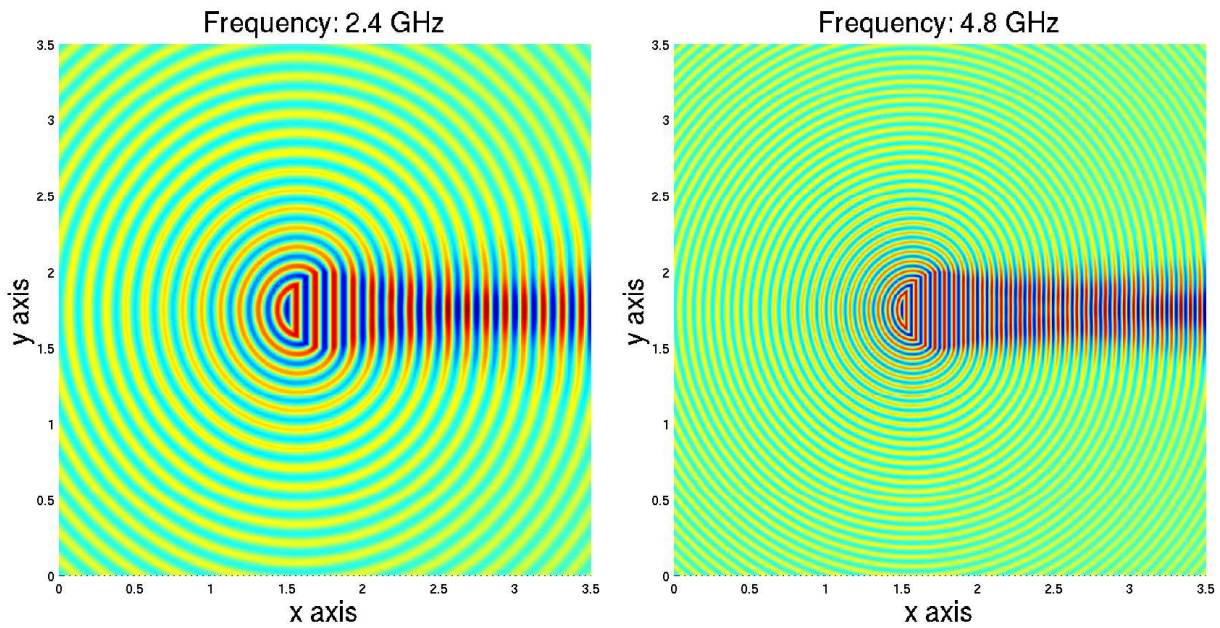


Figure 13: A top view of the computed solution (real part) for a harmonic planar wave with frequency  $f = 2.4$  GHz and  $L = 0.125$ m (left), and for a harmonic planar wave with frequency  $f = 4.8$  GHz and  $L = 0.0625$ m (right).

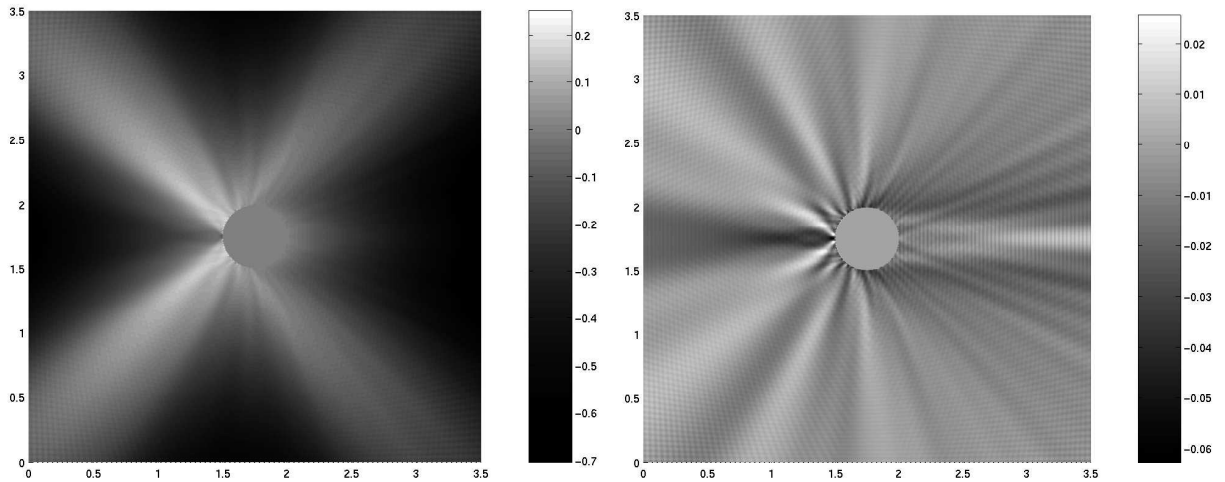


Figure 14: A linear gray scale image of the phase error in radians (left) and the amplitude error (right) over the square domain  $[0, 3.5] \times [0, 3.5]$ .

## 9 Conclusions and Future Work

In this paper we have applied a distributed Lagrange multiplier based fictitious domain method to the solution of the two dimensional Maxwell's equations in the exterior of a domain  $\omega$  with a perfectly conducting condition on the boundary of  $\omega$ . Such a method was applied to the solution of the two dimensional wave equation in [5]. Thus, in this paper we have extended the application of the distributed multiplier to electromagnetic waves. The idea behind the fictitious domain method is to extend the electromagnetic solution inside the obstacle and enforce the perfectly conducting condition on the boundary of the obstacle via the introduction of a distributed Lagrange multiplier. This distributed multiplier is defined on the boundary of the obstacle as well as in the interior of the obstacle.

After presenting our fictitious domain formulation, we have derived energy identities to demonstrate the wellposedness and stability requirements of the method. An interesting fact is that the stability condition is the same as in the case of the problem without an obstacle. We have presented numerical computations which show that our fictitious domain method is more accurate than the finite difference approach. Even though the method remains first order accurate with respect to the mesh step size, the error is much better as compared to the staircase approximation of a the corresponding finite difference scheme. Thus, this paper provides a simple and much more accurate alternative to the popular FDTD method.

We have focused our study on the two dimensional TM mode of Maxwell's equations. In the future we will extend this approach to the TE mode in two dimensions as well as to the full three dimensional Maxwell's equations.

## 10 Acknowledgments

The authors would like to thank Dr. H. T. Banks for his support and encouragement of the first author. This material is based on work supported in part by the Department of Energy under Contract Nos. 03891-001-99-4G, 74837-001-03 49, and/or 86192-001-04 49 from the Los Alamos National Laboratory, and in part by the U.S. Air Force office of Scientific Research under grants AFOSR F49620-01-1-0026 and AFOSR FA9550-04-1-0220.

## References

- [1] J. C. ADAM, A. G. SERVENIERE, J.-C. NÉDÉLEC, AND P.-A. RAVIART, *Study of an implicit scheme for integrating Maxwell's equations*, Comput. Methods Appl. Mech. Engrg., 22 (1980), pp. 327–346.

- [2] C. ATAMIAN AND P. JOLY, *Une analyse de la méthode des domaines fictifs pour le probleme de Hemholtz extérieur*, Tech. Rep. 1378, INRIA, 1991.
- [3] E. BÉCACHE AND P. JOLY, *On the analysis of Berenger's perfectly matched layers for Maxwell's equations*, Math. Model. Numer. Anal., 36 (2002), pp. 87–119.
- [4] V. BOKIL AND M. BUKSAS, *Comparision of a finite difference and a mixed finite element formulation of the uniaxial perfectly matched layer*, tech. rep., CRSC, North Carolina State University, 2006.
- [5] V. A. BOKIL AND R. GLOWINSKI, *An operator splitting scheme with a distributed Lagrange multiplier based fictitious domain method for wave propagation problems*, J. Comput. Phys., 205 (2005), pp. 242–268.
- [6] M. O. BRISTEAU, V. GIRAULT, R. GLOWINSKI, T. W. PAN, J. PÉRIAUX, AND Y. XIANG, *On a fictitious domain method for flow and wave problems*, in Domain Decomposition Methods in Sciences and Engineering, R. Glowinski, ed., 1997, pp. 361–386.
- [7] F. COLLINO, S. GARCÉS, AND P. JOLY, *A fictitious domain method for conformal modeling of the perfect electric conductors in the FDTD method*, IEEE Trans. Antennas Propagat., 46 (1998), pp. 1519–1526.
- [8] F. COLLINO, P. JOLY, AND F. MILLOT, *Fictitious domain method for unsteady problems: Application to electromagnetic scattering*, J. Comput. Phys., 138 (1997), pp. 907–938.
- [9] W. DAHMEN, T. KLINT, AND K. URBAN, *On fictitious domain formulations for Maxwell's equations*, Found. Comput. Math., 3 (2003), pp. 135–160.
- [10] R. DAUTRAY AND J.-L. LIONS, *Mathematical Analysis and Numerical Methods for Science and Technology*, vol. 3, Springer-Verlag, Berlin Heidelberg, 1990.
- [11] G. DUVAUT AND J.-L. LIONS, *Inequalities in Mechanics and Physics*, Springer-Verlag, New York, 1976.
- [12] S. GARCÉS, *Une méthode de domaines fictifs pour la modélisation des structures rayonnantes tridimensionnelles*, PhD thesis, Ecole Nationale Supérieure de Aéronautique et de Espace, 1997.
- [13] S. D. GEDNEY, *An anisotropic perfectly matched layer absorbing media for the truncation of FDTD lattices*, IEEE Trans. Antennas Propagat., 44 (1996), pp. 1630–1639.

- [14] V. GIRAULT AND R. GLOWINSKI, *Error analysis of a fictitious domain method applied to a Dirichlet problem*, Japan J. Indust. Appl. Math., 12 (1995), pp. 487–514.
- [15] R. GLOWINSKI AND P. LETALLEC, *Augmented Lagrangian and Operator Splitting Methods in Nonlinear Mechanics*, SIAM, Philadelphia, 1989.
- [16] R. GLOWINSKI, T. W. PAN, AND J. PÉRIAUX, *A fictitious domain method for Dirichlet problem and applications*, Comput. Methods Appl. Mech. Eng., 111 (1994), pp. 283–303.
- [17] F. KIKUCHI, *Mixed and penalty formulations for finite element analysis of an eigenvalue problem in electromagnetism*, Comput. Methods Appl. Mech. Engrg., 64 (1987), pp. 509–521.
- [18] R. LEIS, *Initial Boundary Value Problems in Mathematical Physics*, John Wiley, New York, 1988.
- [19] G. I. MARCHUK, Y. A. KUZNETSOV, AND A. M. MATSOKIN, *Fictitious domain and domain decomposition methods*, Sov. J. Numer. Anal. Math. Modelling, 1 (1986), pp. 3–35.
- [20] P. MONK, *A comparison of three mixed methods for the time-dependent Maxwell's equations*, SIAM J. Sci. Stat. Comput., 13 (1992), pp. 1097–1122.
- [21] ———, *An analysis of Nédélec's method for the spatial discretization of Maxwell's equations*, J. Comput. Appl. Math., 47 (1993), pp. 101–121.
- [22] P. MONK AND K. PARROTT, *Analysis of finite element time domain methods in electromagnetic scattering*, Tech. Rep. 96/25, Oxford University Computing Laboratory, Numerical Analysis Group, Oxford, England OX1 3QD, December 1996.
- [23] A. NACHMAN, *Minireview: A brief perspective on computational electromagnetics*, J. Comput. Phys., 126 (1996), pp. 237–239.
- [24] P. A. RAVIART AND J. M. THOMAS, *A mixed finite element method for 2nd order elliptic problems*, in Proc. of Math. Aspects on the Finite Element Method, I. Galligani and E. Magenes, eds., vol. 606 of Lecture Notes in Mathematics, Springer-Verlag, 1977, pp. 292–315.
- [25] Z. S. SACKS, D. M. KINSLAND, R. LEE, AND J. F. LEE, *A perfectly matched anisotropic absorber for use as an absorbing boundary condition*, IEEE Trans. Antennas Propagat., 43 (1995), pp. 1460–1463.

- [26] V. K. SAUL'EV, *Solution of certain boundary-value problems on high-speed computers by the fictitious-domain method*, Sibirsk. Mat. Ž., 4 (1963), pp. 912–925.
- [27] A. TAFLOVE, *Advances in Computational Electrodynamics: The Finite-Difference Time-Domain method*, Artech House, Norwood, MA, 1998.